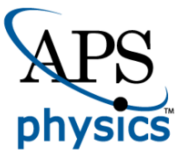

Accuracy of the adiabatic-impulse approximation for closed and open quantum systems

Michael Tomka, Lorenzo Campos Venuti, and Paolo Zanardi

Phys. Rev. A **97**, 032121 — Published 22 March 2018

DOI: 10.1103/PhysRevA.97.032121

Accuracy of the adiabatic-impulse approximation for closed and open quantum systems

Michael Tomka,[1,2,*] Lorenzo Campos Venuti,[1,2] and Paolo Zanardi[1,2]

[1] *Department of Physics & Astronomy, University of Southern California, Los Angeles, California 90089, USA*
[2] *Center for Quantum Information Science & Technology, University of Southern California, Los Angeles, California 90089, USA*

(Dated: December 12, 2017)

We study the adiabatic-impulse approximation (AIA) as a tool to approximate the time evolution of quantum states, when driven through a region of small gap. Such small gap regions are a common situation in adiabatic quantum computing and having reliable approximations is important in this context. The AIA originates from the Kibble-Zurek theory applied to continuous quantum phase transitions. The Kibble-Zurek mechanism was developed to predict the power-law scaling of the defect density across a continuous quantum phase transition. Instead here, we quantify the accuracy of the AIA via the trace norm distance with respect to the exact evolved state. As expected, we find that for short times/fast protocols, the AIA outperforms the simple adiabatic approximation. However, for large times/slow protocols, the situation is actually reversed and the AIA provides a worse approximation. Nevertheless, we found a variation of the AIA that can perform better than the adiabatic one. This counter-intuitive modification consists in crossing *twice* the region of small gap. Our findings are illustrated by several examples of driven closed and open quantum systems.

I. INTRODUCTION

Progress made during the last thirty years in the field of atomic and molecular optics, in experiments with trapped ions, and in cavity and circuit quantum electrodynamics, has drastically improved the experimental control over the dynamics of quantum many-body systems. These experimental implementations of controllable quantum systems [1–3], opened the possibility to use quantum physics towards the realization of quantum technologies like quantum computers [4–6] and quantum simulators [7]. Among the different approaches to quantum computing, the adiabatic one is recently attracting a lot of attention [8–13]. The basic idea behind adiabatic quantum computation is that the ground-state of certain quantum systems can encode the solution to a mathematical problem, e.g., the solution of a minimization problem. The algorithm is to start with a simple Hamiltonian whose ground-state can easily be prepared. In order to get from this easy available ground-state, to the target ground-state, encoding the solution of the minimization problem, one adiabatically evolves the simple Hamiltonian to the desired complicated Hamiltonian. According to the adiabatic theorem, the system remains in the same level, if the total evolution time is large enough, such that the system ends up being in the state describing the solution of the minimization problem.

It is clearly very important to understand the precise mode of operation of such an adiabatic quantum algorithm, in order to obtain faithful results and to understand the limit of its performance. Key problems are controlling the precision of the initial ground-state preparation, having full control over the system's parameters and understanding the main features that control the adiabatic evolution of the quantum many-body system, i.e., being aware of when the energy gap, the energy difference between the ground-state and the first excited-state, becomes small, as well as the effects of dissipation and decoherence. Examples where the adiabatic dynamics can be analyzed in full details are rare and only possible for very small quantum systems, therefore to understand and fully quantify the performance of adiabatic quantum computers one needs to relay on approximation methods.

Consequently, in the present work we study the proficiency of the adiabatic-impulse approximation (AIA) to estimate the time evolution of quantum states. The idea behind the AIA is that the time evolution can approximately be divided in an adiabatic and an impulse stage (the impulse stage is sometimes also called sudden or diabatic stage). During the adiabatic stage the external changes are slow compared to the *internal time scale* of the system, such that the adiabatic approximation becomes appropriate. Conversely, in the impulse region the external changes happen so fast that the state has no time to adjust itself, and the impulse approximation is a good one. The difficulty of the AIA lies in the determination of the precise internal time scale of the problem, and/or in the identification of the switching instants: adiabatic to impulse and vice versa. Hence, the paradigmatic situation where the AIA can be applied, appears when the system is driven across a quantum critical point.

Damski [14] applied the AIA to study the quantum dynamics of the excitations in the Landau-Zener model. It was pointed out, that the AIA is based on the Kibble-Zurek (KZ) theory of non-equilibrium classical phase transitions [14–16]. The KZ theory provides one way to determine this internal time scale, namely, assuming that it is given by the inverse gap. This recipe fixes the time scale apart from a dimensionless constant, that traditionally is fixed by comparing the approximation of the

* mtomka@usc.edu

density of excitation to the analytical expression [14–16]. In this paper we will carefully examine different strategies to fix this internal time scale, which allows us to estimate the adiabatic-impulse switching times. The accuracy of the resulting AIA is evaluated by considering the trace norm distance between the obtained approximation and the numerically performed exact evolution.

The scaling prediction of the KZ mechanism have been confirmed in a series of works [17]. However we note, that the same scaling predictions can be obtained without resorting to the AIA [18, 19].

The paper is organized as follows. Section II gives a short review of the AIA in closed systems. Then it is applied to approximate the time evolution of two paradigmatic examples, namely the Landau-Zener (LZ) model and the transverse field Ising (TFI) model. The AIA method is evaluated by studying the distance between the exact evolved state, which is computed numerically, and the one obtained by the AIA. In Sec. III we will extend the AIA to approximate the time evolution of open quantum systems. More specifically, we consider a dissipative quantum system, where the dynamics are described by a time-dependent Lindblad master-equation in the Davies form. As an example, we consider a single qubit coupled to a thermal bath and study the AIA as in the closed case. A brief summary is presented in the concluding Sec. IV. Appendixes A and B give some details on the adiabatic intertwiner that evolves the states corresponding to the eigenvectors of the Liouvillian with zero eigenvalue and the full adiabatic intertwiner that evolves all the eigenvectors together, respectively. In Appendix C we derive the eigenvalues and eigenvectors of the Liouvillian describing the single qubit coupled to a thermal bath and Appendix D shows the corresponding evolution equations. Finally, we note that throughout the text we set $\hbar = 1$.

II. ADIABATIC-IMPULSE APPROXIMATION IN CLOSED SYSTEMS

In this section, we examine the accuracy of the adiabatic-impulse approximation (AIA) method for the time evolution of isolated quantum systems, that are driven through a region of minimal gap. First, we will review the basic ideas of the AIA for closed systems. We evaluate the AIA by computing the distance between the fully evolved state, obtained by numerically propagating the time-dependent Schrödinger equation, and the state obtained by the AIA. As a comparison we use the simple adiabatic approximation, and consider the distance between the fully evolved state and the adiabatic approximation. This will be illustrated by the examples of the Landau-Zener model (avoided level crossing) and the transverse field Ising model (quantum phase transition).

A. General Setting

Let us consider a closed quantum system described by a time-dependent Hamiltonian $\hat{\mathrm{H}}(t)$, whose instantaneous eigenstates and eigenenergies are and given by

$$\hat{\mathrm{H}}(t)|\psi_n(t)\rangle = E_n(t)|\psi_n(t)\rangle, \tag{1}$$

with $n = 1, 2, \ldots, \dim \mathcal{H}$, where $\dim \mathcal{H}$ is the dimension of the Hilbert space $\mathcal{H}$. Just for simplicity we consider the Hamiltonian to be non-degenerate. We label the ground-state by $n = 1$, the first-excited state by $n = 2$, and so on. Further, we assume that the time-dependence enters through a single parameter denoted by $\lambda(t)$.

We focus on dynamics that include both an adiabatic and an impulse regime, e.g., the crossing of a quantum critical point. The unitary time evolution of a closed quantum system is adiabatic, when the system initialized in an eigenstate $|\psi_m(t_i)\rangle$ will remain in it $|\psi_m(t)\rangle$ for all $t \in [t_i, t_f]$, where t_i and t_f denote the initial and the final time, respectively. A "folklore" condition that the evolution is adiabatic can be given by

$$\max_{t\in[t_i,t_f]} \frac{|\langle\psi_n|\partial_t\hat{\mathrm{H}}|\psi_m\rangle|}{|E_n - E_m|} \ll \min_{t\in[t_i,t_f]} |E_n - E_m|, \quad \forall\, n \neq m, \tag{2}$$

see [20]. In the region where the gap becomes minimal, the time evolution becomes diabatic (impulse regime). During the impulse regime the system can no longer adjusts to the external changes in the Hamiltonian and therefore its state is effectively frozen. The time evolution of the wave-function is thus approximated by a sudden jump through this regime, in other words, no changes in the wave-function occur.

Our protocol will be the following, we initialize the system at $t_i = 0$ in the ground-state $|\psi_0(0)\rangle$ and then tune the parameter $\lambda(t)$ from its initial value $\lambda_i = \lambda(0)$ to its final value $\lambda_f = \lambda(t_f)$. We assume that the gap, $\Delta \equiv E_1 - E_0$, will be minimal at a single instant in time. Within the AIA the evolution is assumed to be adiabatic until the instant τ_- and again adiabatic after τ_+ and the minimum of the gap occurs within the interval $[\tau_-, \tau_+]$. During the interval $[\tau_-, \tau_+]$ the state of the system is assumed not change, it suddenly jumps from τ_- to τ_+.

The Kibble-Zurek argument used in [14–16] presumes the impulse instants $\tau_\pm$ to be determined by the time, when the transition time, $|\frac{\lambda}{\partial_t\lambda}|$, is equal to the inverse gap, $1/\Delta$,

$$\left|\frac{\lambda(t)}{\partial_t\lambda(t)}\right|_{t=\tau} = \frac{1}{\Delta(\lambda(\tau))}. \tag{3}$$

This equation is the adaptation from the so-called Kibble-Zurek theory of topological defect production during classical phase transition [21–25], where the corresponding crossover time is determined by the condition $t_{\mathrm{rel}}(\tau) = \tau$, t_{rel} being the relaxation time scale of the system. In order to adapt the KZ theory to quantum systems, the identification $t_{\mathrm{rel}} = 1/\Delta$ was made in [14],

to obtain Eq. (3). Within the following examples, the Landau-Zener model and the transverse field Ising model, we will examine, if the condition (3) faithfully estimates the impulse instants or if one needs to find a more refined estimate to improve the AIA.

The fully time evolved state, $|\psi(t)\rangle$, is given by the solution of the Schrödinger equation, $\partial_t|\psi(t)\rangle = -i\,\hat{\mathrm{H}}(t)|\psi(t)\rangle$, which can formally be written as

$$|\psi(t_f)\rangle = \overleftarrow{\mathrm{T}}\mathrm{exp}\left[\int_0^{t_f} dt(-i)\hat{\mathrm{H}}(t)\right]|\psi(0)\rangle, \tag{4}$$

where $\overleftarrow{\mathrm{T}}$ is the time-ordering operator, which arranges operators in a chronological order with time increasing from right to left. We note, that for all the examples considered here we computed the time evolution numerically.

The adiabatic approximation of the state $|\psi(t_f)\rangle$ is given by

$$|\psi_{\mathrm{adi}}(t_f)\rangle = \hat{\mathrm{U}}(t_f,0)|\psi(0)\rangle, \tag{5}$$

where $\hat{\mathrm{U}}(t_f,0) = \sum_n e^{i\phi_n(t_f,0)}|\psi_n(t_f)\rangle\langle\psi_n(0)|$, is the full adiabatic intertwiner [26], and $\phi_n(t_f,0) = -\delta_n(t_f,0) + \gamma_n(t_f,0)$ is the sum of the dynamic phase of the n-th eigenstate $\delta_n(t_f,0) = \int_0^{t_f} E_n(t)\,dt$ and the corresponding geometric phase $\gamma_n(t_f,0) = \int_0^{t_f} i\,\langle\psi_n|\partial_t|\psi_n\rangle\,dt$. If the initial state is the ground-state $|\psi(0)\rangle = |\psi_1(0)\rangle$, the last equation reduces to

$$|\psi_{\mathrm{adi}}(t_f)\rangle = e^{i\phi_1(t_f,0)}|\psi_1(t_f)\rangle. \tag{6}$$

A more refined approximation might be given by the AIA, where the evolution is adiabatic before τ_-, $(0 < t < \tau_-)$, and again after τ_+, $(\tau_+ < t < t_f)$, but it suddenly jumps from τ_- to τ_+. Consequently, within the AIA scheme the time evolved state is approximated by

$$|\psi_{\mathrm{aia}}(t_f)\rangle = \hat{\mathrm{U}}(t_f,\tau_+)\,\hat{1}\,\hat{\mathrm{U}}(\tau_-,0)|\psi(0)\rangle, \tag{7}$$

and which for $|\psi(0)\rangle = |\psi_1(0)\rangle$ reduces to

$$|\psi_{\mathrm{aia}}(t_f)\rangle = \sum_n e^{i\phi_n(t_f,\tau_+)}e^{i\phi_0(\tau_-,0)}\langle\psi_n(\tau_+)|\psi_1(\tau_-)\rangle|\psi_n(t_f)\rangle. \tag{8}$$

As a measure to quantify the adiabatic approximation and the AIA, we use the distance between two given wave-functions, $|\psi\rangle \in \mathcal{H}$ and $|\phi\rangle \in \mathcal{H}$,

$$\mathrm{d}[|\psi\rangle,|\phi\rangle] = \sqrt{1-|\langle\psi|\phi\rangle|^2}, \tag{9}$$

which we note is defined in terms of the fidelity $\mathcal{F}(|\psi\rangle,|\phi\rangle) = |\langle\psi|\phi\rangle|^2$. The distance between the fully evolved state $|\psi(t_f)\rangle$ and the adiabatic approximation is denoted by $\mathrm{d}_{\mathrm{adi}}(t_f) = \mathrm{d}[|\psi(t_f)\rangle,|\psi_{\mathrm{adi}}(t_f)\rangle]$, while the distance between the fully evolved state and the one obtained by the AIA is labeled $\mathrm{d}_{\mathrm{aia}}(t_f) = \mathrm{d}[|\psi(t_f)\rangle,|\psi_{\mathrm{aia}}(t_f)\rangle]$.

B. Landau-Zener model

As a first example, we consider the Landau-Zener model, described by the Hamiltonian

$$\hat{\mathrm{H}}_{\mathrm{LZ}}(t) = x(t)\hat{\sigma}^x + z(t)\hat{\sigma}^z = \begin{pmatrix} z(t) & x(t) \\ x(t) & -z(t)\end{pmatrix}, \tag{10}$$

where $\hat{\sigma}^x$ and $\hat{\sigma}^z$ are the usual Pauli matrices, and $|\varphi_1\rangle = (1,0)^T$, $|\varphi_2\rangle = (0,1)^T$, denote the eigenstates of $\hat{\sigma}^z$. The parameter x characterizes the coupling between the two levels and z the detuning. The eigenenergies of this system are $E_{1,2} = \mp b$, where we defined $b \equiv \sqrt{x^2+z^2}$, and the corresponding eigenstates read

$$|\psi_{1,2}(t)\rangle = \mp\sqrt{\frac{b\mp z}{2\,b}}|\varphi_1\rangle + \sqrt{\frac{b\pm z}{2\,b}}|\varphi_2\rangle. \tag{11}$$

We assume the protocol, where x is constant in time, $z(t)$ changes linear, $z(t) = z_i + (z_f - z_i)\,t/t_f$, with $t \in [0,t_f]$, and the system is initially prepared in the ground-state, $|\psi(0)\rangle = |\psi_1(0)\rangle$. For the initial point, z_i, we choose a negative value, and for the final point, z_f, a positive value, such that the protocol passes the avoided level crossing at $z = 0$. Let us note, that our protocol is similar to the paradigmatic Landau-Zener problem [27–30], however, in the Landau-Zener problem one has, $z(t) = t/t_f$, with $t \in [-\infty,\infty]$. The Schrödinger equation, $\partial_t|\psi\rangle = -i\,\hat{\mathrm{H}}_{\mathrm{LZ}}|\psi\rangle$, written in the fixed basis, $|\psi(t)\rangle = \sum_{i=1}^2 c_i(t)|\varphi_i\rangle$, becomes

$$i\,\partial_t c_1 = z(t)\,c_1 + x\,c_2, \qquad i\,\partial_t c_2 = x\,c_1 - z(t)\,c_2, \tag{12}$$

with the initial conditions given by the ground-state

$$c_1(0) = -\sqrt{\frac{b_i - z_i}{2\,b_i}}, \qquad c_2(0) = \sqrt{\frac{b_i+z_i}{2\,b_i}}, \tag{13}$$

where $b_i \equiv \sqrt{x^2+z_i^2}$. This system can be solved in terms of parabolic cylinder functions [31], and therefore provides a convenient benchmark to study the accuracy of the adiabatic-impulse approximation.

We begin by studying the simple adiabatic approximation of the time evolved state, $|\psi(t_f)\rangle$, which is given by

$$|\psi_{\mathrm{adi}}(t_f)\rangle = e^{-i\delta_1(0,t_f)}|\psi_1(t_f)\rangle, \tag{14}$$

and where the dynamical phase of the ground-state reads

$$\delta_1(0,t_f) \equiv \int_0^{t_f} E_1(t)\,dt = \frac{t_f}{2\,\delta z}\,\left[b\,z + x^2\log(z+b)\right]\Big|_{z_i}^{z_f}, \tag{15}$$

with $\delta z \equiv z_f - z_i$. Note that there is no Berry phase, $\gamma_1(0,t_f) = \int_0^{t_f} dt\,i\langle\psi_1|\partial_t|\psi_1\rangle = 0$, since the Landau-Zener Hamiltonian is real. In Fig. 1 we plot $\mathrm{d}_{\mathrm{adi}}(t_f)$ on a logarithmic scale for $z_i = -1, z_f = 1$ and $x = 0.1$. It can be seen that for large t_f the distance decreases with t_f^{-1}, as expected by the adiabatic theorem [32].

Next, we analyze the first-order correction in $1/t_f$ of the adiabatic approximation, which can be expressed by

$$|\psi_{\mathrm{adi},1}(t_f)\rangle = N^{-1}\left[|\psi_{\mathrm{adi}}(t_f)\rangle + \frac{1}{t_f}|\psi^{(1)}_{\mathrm{adi}}(t_f)\rangle\right], \quad (16)$$

where

$$\begin{aligned}|\psi^{(1)}_{\mathrm{adi}}(t_f)\rangle &= i\,e^{-i\delta_1(0,t_f)}J_{21}(t_f)|\psi_1(t_f)\rangle \\ &- i\,e^{-i\delta_1(0,t_f)}M_{21}(t_f)|\psi_2(t_f)\rangle \\ &+ i\,e^{-i\delta_2(0,t_f)}M_{21}(0)|\psi_2(t_f)\rangle, \quad (17)\end{aligned}$$

and where we used the notations

$$J_{21}(t) = t_f\int_0^t \frac{|\langle\psi_2|\partial_{t'}\hat{\mathrm{H}}_{\mathrm{LZ}}|\psi_1\rangle|^2}{(E_2-E_1)^3}dt', \quad (18)$$

$$M_{21}(t) = t_f\frac{\langle\psi_2|\partial_t\hat{\mathrm{H}}_{\mathrm{LZ}}|\psi_1\rangle}{(E_2-E_1)^2}. \quad (19)$$

The dynamical phase of the excited-state is given by $\delta_2(0,t_f) = -\delta_1(0,t_f)$, and the normalization reads $N^2 = 1 + \langle\psi^{(1)}_{\mathrm{adi}}(t_f)|\psi^{(1)}_{\mathrm{adi}}(t_f)\rangle$. For a derivation of Eq. (16) see Ref. [33]. The distance between the exactly evolved state and the first order correction, $\mathrm{d}_{\mathrm{adi},1}(t_f) = \mathrm{d}[|\psi(t_f)\rangle, |\psi_{\mathrm{adi},1}(t_f)\rangle]$, is also plotted in Fig. 1. Correctly, the distance $\mathrm{d}_{\mathrm{adi},1}(t_f)$ decreases with, $2.06\ t_f^{-2.03}$, for large t_f, and hence gets much smaller than $\mathrm{d}_{\mathrm{adi}}(t_f)$. The power law t_f^{-2} is predicted by the adiabatic theorem, namely the distance between the n-th order correction and the fully evolved state is of the order $(1/t_f)^{n+1}$ [34, 35].

Let us now turn to the AIA and study how its accuracy compares to the adiabatic expansion. The time evolved state within the AIA for our Landau-Zener model reduces to

$$|\psi_{\mathrm{aia}}(t_f)\rangle = \sum_{j=1}^{2} e^{-i\delta_j(\tau_+,t_f)}e^{i\delta_1(0,\tau_-)}\langle\psi_j(\tau_+)|\psi_1(\tau_-)\rangle|\psi_j(t_f)\rangle, \quad (20)$$

where the Berry phase of the excited-state is also zero, due to the fact that the Hamiltonian is real. As mentioned above, the difficulty of the AIA is the determination of the time instants τ_- and τ_+, where the evolution switches from adiabatic to impulse and back from the impulse regime to adiabatic, respectively. In the following we will discuss different scenarios providing the instants $\tau_\pm$.

1. *Switching instants $\tau_{1,\pm}$: standard Kibble-Zurek argument*

First, we consider the Kibble-Zurek argument, as proposed in [14–16]. The argument is based on the heuristic, that sufficiently close to the critical point, here the avoided level crossing, the dynamics appears to be

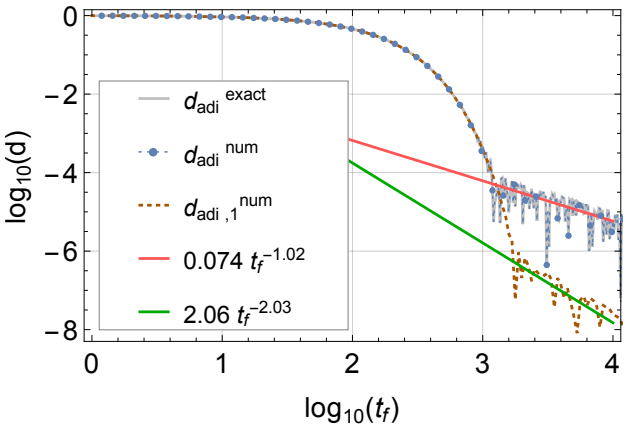

Figure 1. (Color online) We plot $\mathrm{d}_{\mathrm{adi}}$ and $\mathrm{d}_{\mathrm{adi},1}$ as a function of the total evolution time t_f for $z_i = -1$, $z_f = 1$ and $x = 0.1$. The gray solid line corresponds to the distance between the adiabatic approximation $|\psi_{\mathrm{adi}}(t_f)\rangle$ and the time evolved state $|\psi(t_f)\rangle$ obtained by in terms of the parabolic cylinder functions, denoted by $\mathrm{d}_{\mathrm{adi}}{}^{\mathrm{exact}}$. To check our numerical procedure for solving the Schrödinger equation we plotted also $\mathrm{d}_{\mathrm{adi}}{}^{\mathrm{num}}$ (blue dashed line with circles), which corresponds to the distance between the adiabatic approximation $|\psi_{\mathrm{adi}}(t_f)\rangle$ and the time evolved state $|\psi(t_f)\rangle$ found by numerically solving Eq. (12). We see a perfect agreement between the exact and the numerically obtained distance and therefore use the same numerical procedure for the other examples in the text. The orange dotted line shows the distance between the first order correction to the adiabatic approximation and the fully time evolved state, $\mathrm{d}_{\mathrm{adi},1}$.

"frozen". The system's dynamics has not enough time to adjust to the changes of the external parameters, due to the smallness of the gap $\Delta \equiv E_2 - E_1 = 2b$. According to the Kibble-Zurek argument this critical slowing down occurs, when the inverse of the gap is on the order of the inverse rate of change of the external parameter, therefore $\tau_\pm$ are determined by

$$\frac{1}{\Delta(\tau)} = \left|\frac{z(t)}{\partial_t z(t)}\right|_{t=\tau}. \quad (21)$$

This equation has two real solutions

$$\tilde{\tau}_{1,\pm} = -\frac{z_i}{\delta z}t_f \pm \frac{x}{\sqrt{2}\,\delta z}t_f\sqrt{-1+\sqrt{1+\left(\frac{\delta z}{x^2}\frac{1}{t_f}\right)^2}}. \quad (22)$$

We note that the instants $\tau_\pm$ have to be positive and smaller than or equal to the total evolution time t_f, since for our protocol $t \in [0, t_f]$, and therefore we find

$$\tau_{1,\pm} = \begin{cases} \begin{cases} t_f \\ 0 \end{cases}, & 0 < t_f < \frac{1}{2}\frac{\delta z}{z_f\sqrt{x^2+z_f^2}} \\ \tilde{\tau}_{1,\pm}, & \frac{1}{2}\frac{\delta z}{z_f\sqrt{x^2+z_f^2}} < t_f < \infty \end{cases}. \quad (23)$$

In Fig. 2 we plot the resulting impulse interval, $\Delta\tau_1 \equiv \tau_{1,+} - \tau_{1,-}$, as a function of t_f for $z_i = -1$, $z_f = 1$

and $x = 0.1$ (red dotted line). We note, the interval $\Delta\tau_1$ reaches the constant value $1/x$ in the limit of t_f approaching infinity. The distance between the AIA $|\psi_{\text{aia}-1}(t_f)\rangle$ and the fully evolved state (numerical solution of Eq. (12)), $\mathrm{d}_{\text{aia}-1}(t_f) = \mathrm{d}[|\psi(t_f)\rangle, |\psi_{\text{aia}-1}(t_f)\rangle]$, using the transition times $\tau_{1,\pm}$, is plotted in Fig. 3 (red dotted line). One can see that the AIA provides a slightly better approximation to the fully evolved state than the adiabatic expansion only for very small t_f. For large t_f we find, $\mathrm{d}_{\text{aia}-1}(t_f) = 99.08\ t_f^{-1}$, providing a much worse approximation than the adiabatic one, which is $\mathrm{d}_{\text{adi}}(t_f) = 0.074\ t_f^{-1}$. We attribute this discrepancy to the overestimation of the impulse interval, given by the Kibble-Zurek argument (12), in the adiabatic limit ($t_f \to \infty$).

2. *Switching instants $\tau_{2,\pm}$: modified Kibble-Zurek argument*

Consequently, as a second scenario we consider a slight modification of the Kibble-Zurek argument. Namely, we replace the inverse rate of change of the external parameter $z/\partial_t z$ in Eq. (21) by the inverse rate of change of the Hamiltonian. The resulting condition becomes

$$\frac{1}{\Delta(\tau)} = \left.\frac{\|\hat{\mathrm{H}}_{\mathrm{LZ}}(t)\|_\infty}{\|\partial_t \hat{\mathrm{H}}_{\mathrm{LZ}}(t)\|_\infty}\right|_{t=\tau}, \tag{24}$$

where $\|\cdot\|_\infty$ is the operator norm defined by $\|\hat{\mathrm{O}}\|_\infty \equiv \max_i \mathrm{s}_i(\hat{\mathrm{O}})$, and $\mathrm{s}_i(\hat{\mathrm{O}})$ are the singular values of $\hat{\mathrm{O}}$, i.e., eigenvalues of $|\hat{\mathrm{O}}| \equiv \sqrt{\hat{\mathrm{O}}^\dagger \hat{\mathrm{O}}}$. The two real solutions of Eq. (24) are

$$\tilde{\tau}_{2,\pm} = -\frac{z_i}{\delta z} t_f \pm \frac{x}{\sqrt{2}\,\delta z} t_f \sqrt{-2 + \frac{\delta z}{x^2}\frac{1}{t_f}}, \tag{25}$$

and hence we obtain for the adiabatic-impulse switching times

$$\tau_{2,\pm} = \begin{cases} \begin{cases} t_f \\ 0 \end{cases}, & 0 < t_f < \frac{1}{2}\frac{\delta z}{x^2+z_i^2} \\ \tilde{\tau}_{2,\pm}, & \frac{1}{2}\frac{\delta z}{x^2+z_i^2} < t_f < \frac{1}{2}\frac{\delta z}{x^2} \\ \frac{t_f}{2}, & \frac{1}{2}\frac{\delta z}{x^2} < t_f < \infty \end{cases}. \tag{26}$$

The corresponding impulse interval reads, $\Delta\tau_2 \equiv \tau_{2,+} - \tau_{2,-}$, and is also shown in Fig. 2 (dashed green line). It vanishes, if $t_f > \delta z/(2x^2)$, and therefore the distance $\mathrm{d}_{\text{aia}-2}(t_f) = \mathrm{d}[|\psi(t_f)\rangle, |\psi_{\text{aia}-2}(t_f)\rangle]$, where the switching times $\tau_{2,\pm}$ are used, recovers the adiabatic approximation at $t_f = \delta z/(2x^2)$ (see Fig. 3 dashed green line with $*$ symbols).

3. *Switching instants $\tau_{3,\pm}$: simple gap condition*

Within the third approach, we consider the time, when the adiabatic approximation fails, as the instant determining the adiabatic-impulse switching times $\tau_\pm$. The simplest and crudest estimate for the adiabatic evolution to be valid, might be given by $t_f \gg 1/\Delta$, as a consequence we propose the simple equation

$$\frac{1}{\Delta(\tau)} = t_f, \tag{27}$$

to determine the time instants when the adiabaticity breaks down. We find the two solutions

$$\tilde{\tau}_{3,\pm} = -\frac{z_i}{\delta z} t_f \pm \frac{x}{\delta z} t_f \sqrt{-1 + \left(\frac{1}{2x}\frac{1}{t_f}\right)^2}, \tag{28}$$

from which we get for the adiabatic-impulse switching times

$$\tau_{3,\pm} = \begin{cases} \begin{cases} t_f \\ 0 \end{cases}, & 0 < t_f < \frac{1}{2}\frac{1}{\sqrt{x^2+z_f^2}} \\ \tilde{\tau}_{3,\pm}, & \frac{1}{2}\frac{1}{\sqrt{x^2+z_f^2}} < t_f < \frac{1}{2x} \\ -\frac{z_i}{\delta z} t_f, & \frac{1}{2x} < t_f < \infty \end{cases}. \tag{29}$$

Figure 2 shows also a plot of, $\Delta\tau_3 \equiv \tau_{3,+} - \tau_{3,-}$ (blue dot-dashed line). In the present case the impulse interval vanishes for $t_f > 1/(2x)$, which is much smaller than in the previous case, and hence the resulting distance $\mathrm{d}_{\text{aia}-3}(t_f) = \mathrm{d}[|\psi(t_f)\rangle, |\psi_{\text{aia}-3}(t_f)\rangle]$, becomes the same as for the adiabatic approximation at $t_f = 1/(2x)$ (see Fig. 3 blue dot-dashed line with $+$ symbols). This scenario does also not provide an improvement of the AIA, since the estimate of the time when the adiabatic approximation fails is by far underestimated.

4. *Switching instants $\tau_{4,\pm}$: "folklore" adiabatic condition*

A more refined estimate for the validity of the adiabatic evolution, if the system is initially prepared in the ground-state, might be provided by

$$\max_{t\in[0,t_f]} \frac{|\langle\psi_2(t)|\partial_t \hat{\mathrm{H}}_{\mathrm{LZ}}(t)|\psi_1(t)\rangle|}{\Delta^2} \ll 1, \tag{30}$$

see [20]. Consequently, we propose the following equation

$$|\langle\psi_2(t)|\partial_t \hat{\mathrm{H}}_{\mathrm{LZ}}(t)|\psi_1(t)\rangle|_{t=\tau} = \Delta(\tau)^2, \tag{31}$$

to determine the adiabatic-impulse switching times. Equation (31) has the two solutions

$$\tilde{\tau}_{4,\pm} = -\frac{z_i}{\delta z} t_f \pm \frac{x}{\sqrt{2}\,\delta z} t_f \sqrt{-2 + \left(\frac{\delta z}{\sqrt{2}\,x^2}\frac{1}{t_f}\right)^{2/3}}, \tag{32}$$

which provides the adiabatic-impulse switching times

$$\tau_{4,\pm} = \begin{cases} \begin{cases} t_f \\ 0 \end{cases}, & 0 < t_f < \frac{1}{4}\frac{x\delta z}{x^2+z_i^2} \\ \tilde{\tau}_{4,\pm}, & \frac{1}{4}\frac{x\delta z}{x^2+z_i^2} < t_f < \frac{1}{4}\frac{\delta z}{x^2} \\ \frac{t_f}{2}, & \frac{1}{4}\frac{\delta z}{x^2} < t_f < \infty \end{cases}. \tag{33}$$

Likewise, we plot the impulse interval, $\Delta\tau_4 \equiv \tau_{4,+} - \tau_{4,-}$, in Fig. 2, which is depicted by the orange solid line. The interval now vanishes for $t_f > \delta z/(4x^2)$, which lies in between the one found by the Kibble-Zurek argument using the Hamiltonian's inverse rate of change and the interval found by the simple adiabaticity breaking argument, $1/\Delta = t_f$. As in the previous case, the resulting distance $\mathrm{d}_{\mathrm{aia}-4}(t_f) = \mathrm{d}[|\psi(t_f)\rangle, |\psi_{\mathrm{aia}-4}(t_f)\rangle]$, recovers the adiabatic approximation, but now at $t_f = \delta z/(4x^2)$. This estimate of the impulse regime does therefore also not show any major improvement of the AIA (solid orange line with circles in Fig. 3).

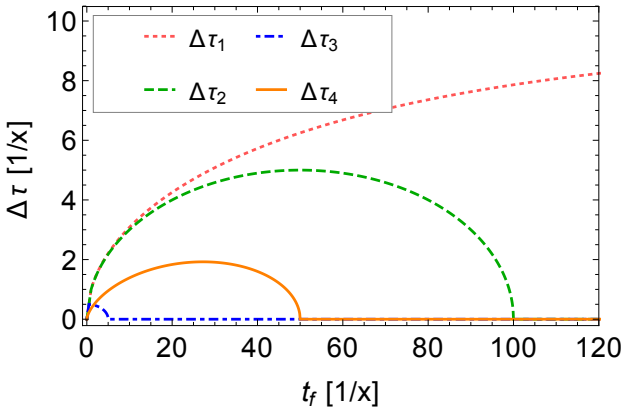

Figure 2. (Color online) We show the impulse interval $\Delta\tau(t_f)$ for $z_i = -1$, $z_f = 1$ and $x = 0.1$, found by the four different scenarios determining the impulse instants $\tau_\pm$. 1) The red dotted line shows $\Delta\tau_1$, obtained by the Kibble-Zurek argument $1/\Delta = z/\partial_t z$. 2) A modified Kibble-Zurek argument $1/\Delta = \|\hat{\mathrm{H}}\| / \|\partial_t \hat{\mathrm{H}}\|$ provided $\Delta\tau_2$, which is shown by the green dashed line. 3) Using the breakdown of the adiabatic theorem as an estimate for the impulse instants, $1/\Delta = t_f$, we found $\Delta\tau_3$, depicted by the blue dot-dashed. Finally, 4) the solid orange line shows $\Delta\tau_4$, given by the adiabaticity condition $|\langle\psi_2|\partial_t\hat{\mathrm{H}}|\psi_1\rangle| = \Delta^2$.

5. *Switching instants $\tau_{\mathrm{opt},\pm}$: optimization*

Neither of the scenarios determining the impulse interval, which we studied above, show an improvement with respect to the simple adiabatic approximation. One might therefore wonder, if there exist an optimal length of the impulse interval, such that the AIA provides a better approximation to the time evolved state than the adiabatic. Consequently, we minimized the distance $\mathrm{d}_{\mathrm{aia}}$, with respect to the impulse interval $\Delta\tau$, where we set $\tau_{\mathrm{opt},\pm} = t_f/2 \pm \Delta\tau/2$. The numerically obtained result of $\Delta\tau_{\mathrm{opt}}(t_f)$ is depicted in Fig. 4, for $z_i = -1$, $z_f = 1$ and $x = 0.1$. The functional form of $\Delta\tau_{\mathrm{opt}}(t_f)$ is similar to $\pi\frac{1}{2}\frac{x^2}{\Delta z}t_f \exp\left(-\pi\frac{1}{2}\frac{x^2}{\Delta z}t_f\right)$, although to our surprise, in the limit of large t_f the optimal interval manifests an oscillatory behavior around zero, which means that it can become negative (Fig. 4 inset). This shows that

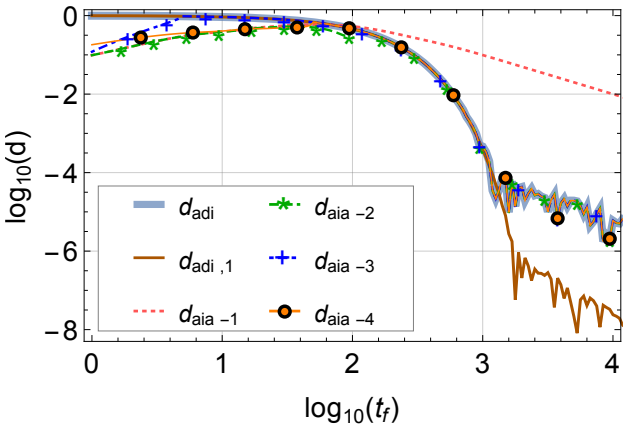

Figure 3. (Color online) The distances between the AIA and the fully evolved state for the four different scenarios considered in the main text is plotted, with $z_i = -1$, $z_f = 1$ and $x = 0.1$. 1) The red dotted line shows $\mathrm{d}_{\mathrm{aia}-1}$, where the transition times $\tau_{1,\pm}$ were used, obtained by the Kibble-Zurek argument $1/\Delta = z/\partial_t z$. 2) A modified Kibble-Zurek argument $1/\Delta = \|\hat{\mathrm{H}}\| / \|\partial_t\hat{\mathrm{H}}\|$ provided $\tau_{2,\pm}$, which was used to calculate $\mathrm{d}_{\mathrm{aia}-2}$ and is shown by the green dashed line with $*$ symbols. 3) Using the breakdown of the adiabatic theorem as an estimate for the impulse instants, $1/\Delta = t_f$, we found $\tau_{3,\pm}$, for which $\mathrm{d}_{\mathrm{aia}-3}$ was calculated and which is depicted by the blue dot-dashed with $+$ symbols. Finally, 4) the solid orange line with circles shows $\mathrm{d}_{\mathrm{aia}-4}$, calculated for the transition times $\tau_{4,\pm}$, given by the adiabaticity condition $|\langle\psi_2|\partial_t\hat{\mathrm{H}}|\psi_1\rangle| = \Delta^2$. As a reference we also plotted the adiabatic distance $\mathrm{d}_{\mathrm{adi}}$ and the next first-order correction $\mathrm{d}_{\mathrm{adi},1}$.

after a certain final time it can become favorable to pass the avoided level crossing adiabatically up to τ_+, then make the "impulse jump" back to τ_-, and finally go again through the avoided level crossing adiabatically. The resulting distance, $\mathrm{d}_{\mathrm{aia}-\mathrm{opt}}(t_f) = \mathrm{d}[|\psi(t_f)\rangle, |\psi_{\mathrm{aia}-\mathrm{opt}}(t_f)\rangle]$, is shown in Fig. 5 (solid purple line). As a comparison, we

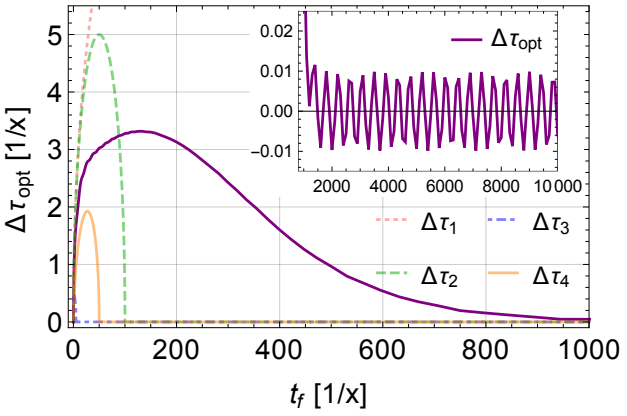

Figure 4. (Color online) A plot of the optimal impulse interval, $\Delta\tau_{\mathrm{opt}}(t_f)$, obtained by numerically minimizing $\mathrm{d}_{\mathrm{aia}}$, for $z_i = -1$, $z_f = 1$ and $x = 0.1$. For comparison we also show the impulse intervals found by the four different scenarios considered in the main text.

also plotted the adiabatic distance $\mathrm{d_{adi}}$ and the first-order correction $\mathrm{d_{adi,1}}$. We can see an overall improvement of the AIA compared to the adiabatic ones. More surprisingly, we find that $\mathrm{d_{aia-opt}}(t_f) = 2.08\ t_f^{-2.03}$, as for the distance obtained by the first order adiabatic correction.

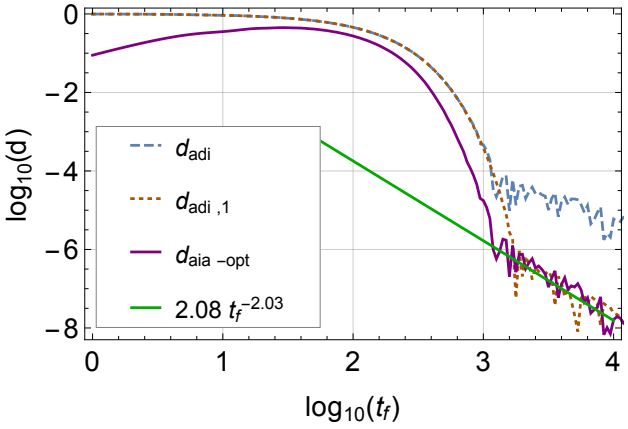

Figure 5. (Color online) We show the minimal distance attainable by the adiabatic-impulse approximation, $\mathrm{d_{aia-opt}}(t_f)$, for $z_i = -1$, $z_f = 1$ and $x = 0.1$. As a reference we also plotted the adiabatic distance $\mathrm{d_{adi}}$ and the first-order correction $\mathrm{d_{adi,1}}$.

C. Transverse Field Ising model

In the following we will study the accuracy of the AIA for a closed quantum many-body system. We consider the illustrative example of the transverse field Ising (TFI) model, whose Hamiltonian is given by

$$\hat{\mathrm{H}}_{\mathrm{TFI}}(t) = \sum_{j=1}^{L} \hat{\sigma}_j^x \hat{\sigma}_{j+1}^x + h(t) \sum_{j=1}^{L} \hat{\sigma}_j^z, \tag{34}$$

where $\hat{\sigma}_j^\alpha$, with $\alpha = x, y, z$, are the Pauli matrices describing the spin on the j-th site of the chain. We assume periodic boundary conditions, $\hat{\sigma}_{L+1}^\alpha = \hat{\sigma}_1^\alpha$, such that the system remains translation invariant. $h(t) \geq 0$ is the transverse magnetic field acting in the z-direction and L gives the total number of spins in the chain. For convenience we choose L to be even. We note that the Jordan-Wigner mapping separates the Hamiltonian into two sub-spaces with an even or an odd number of fermions. In the odd sector, the fermions satisfy periodic boundary conditions, whereas in the even sector they obey anti-periodic boundary conditions. The Jordan-Wigner fermions are always created/destroyed in pairs, and therefore the even/oddness of their number is conserved [36, 37]. Consequently, we can fix a particular fermionic parity (here even), which provides a unique ground-state $|\Psi_{\mathrm{GS}}(h)\rangle$. In the even sector $\hat{\mathrm{H}}_{\mathrm{TFI}}$ can be mapped to a non-interacting spin$-1/2$ model using a Jordan-Wigner followed by a Fourier transformation: $\hat{\mathrm{H}}_{\mathrm{TFI}} = \sum_k \mathbf{c}_k^\dagger \tilde{H}_k \mathbf{c}_k$, where

$$\tilde{H}_k = -\begin{pmatrix} h - \cos k & -i \sin k \\ i \sin k & -(h - \cos k) \end{pmatrix}, \tag{35}$$

with the pseudo-momenta given by

$$k = \pm\frac{1}{2}\frac{2\pi}{L}, \pm\frac{2}{2}\frac{2\pi}{L}, \ldots \pm \left(\frac{L}{2} - \frac{1}{2}\right)\frac{2\pi}{L}, \tag{36}$$

and $\mathbf{c}_k^\dagger = (\hat{\mathrm{c}}_{-k}, \hat{\mathrm{c}}_k^\dagger)$, with $\hat{\mathrm{c}}_k$ being the Fourier transform of the Jordan-Wigner fermions [36–38]. As a consequence, the dynamics of the transverse field Ising model can be decomposed into a collection of uncoupled two-level systems [39, 40]. Finally, through a Bogoliubov transformation, $\hat{\mathrm{H}}_{\mathrm{TFI}}$, can be mapped to a free fermionic Hamiltonian, $\hat{\mathrm{H}}_{\mathrm{TFI}} = \sum_k \epsilon_k (\hat{\gamma}_k^\dagger \hat{\gamma}_k - \frac{1}{2})$, with excitation spectrum

$$\epsilon_k = 2\sqrt{(h - \cos k)^2 + \sin^2 k}, \tag{37}$$

and $\hat{\gamma}_k = \cos\frac{\theta_k}{2}\hat{\mathrm{c}}_k - i \sin\frac{\theta_k}{2}\hat{\mathrm{c}}_{-k}^\dagger$, where $\theta_k = \arctan(\frac{\sin k}{h - \cos k})$. The ground-state of the transverse field Ising model is the vacuum of the Bogoliubov operators, i.e., it is annihilated by all $\hat{\gamma}_k$, and thus reads

$$|\Psi_{\mathrm{GS}}(h)\rangle = \prod_k \left(\cos\frac{\theta_k}{2}|0\rangle_k|0\rangle_{-k} + i \sin\frac{\theta_k}{2}|1\rangle_k|1\rangle_{-k}\right), \tag{38}$$

where $|1\rangle_k = c_k^\dagger|0\rangle_k$. The corresponding ground-state energy is given by $E_{\mathrm{GS}} = -\frac{1}{2}\sum_k \epsilon_k$, which in the thermodynamic limit ($L \to \infty$) becomes

$$E_{\mathrm{GS}} = -\frac{L}{2\pi}\int_0^\pi dk \epsilon_k = -\frac{L}{2\pi} 2(1+h)\mathcal{E}\left[\frac{4h}{(1+h)^2}\right], \tag{39}$$

where $\mathcal{E}[m] \equiv \int_0^{\pi/2} dx \sqrt{1 - m \sin^2 x}$ is the complete elliptic integral. The energy of a single excitation, i.e., a state of the form $|\Psi_q\rangle = \hat{\gamma}_q^\dagger|\Psi_{\mathrm{GS}}\rangle$, is $E_q = \epsilon_q + E_{\mathrm{GS}}$, and therefore the gap reads $\Delta = E_{k_0} - E_{\mathrm{GS}} = \epsilon_{k_0}$, where k_0 is the minimal momentum, defined by the minimum of the excitation energy $\partial_q \epsilon_q = 0$. In the thermodynamic limit we have, $\Delta = |h - 1|$, and thus the gap vanishes at $h_c = 1$, which marks the quantum critical point, where the system undergoes a quantum phase transition from a paramagnetic phase ($h > 1$) to a ferromagnetic phase ($h < 1$).

We will use the schedule, $h(t) = h_i + (h_f - h_i)t/t_f$, with $t \in [0, t_f]$, and the system initially prepared in the ground-state, $|\Psi(t = 0)\rangle = |\Psi_{\mathrm{GS}}(h_i)\rangle$. The starting value h_i, is chosen to be in the ferromagnetic phase, i.e., $h_i < 1$, and the final value, $h_f > 1$, in the paramagnetic phase, such that the quantum critical point is crossed at $h = h_c = 1$.

In Fig. 6 we show the impulse interval $\Delta\tau_1(t_f)$, obtained by the Kibble-Zurek argument $1/\Delta = h/\partial_t h$. Solving this equation yields

$$\tilde{\tau}_{1,\pm} = -\frac{h_i - 1}{\delta h} t_f \pm \frac{1}{\sqrt{2}\sqrt{\delta h}}\sqrt{t_f} \tag{40}$$

with $\delta h \equiv h_f - h_i$, and the resulting impulse interval reads

$$\Delta\tau_{1,\pm} = \begin{cases} t_f, & 0 < t_f < \frac{1}{2}\frac{\delta h}{(h_f-1)^2} \\ \frac{\sqrt{2}}{\sqrt{\delta h}}\sqrt{t_f}, & \frac{1}{2}\frac{\delta h}{(h_f-1)^2} < t_f < \infty \end{cases}. \quad (41)$$

Further, we also plotted the impulse interval $\Delta\tau_2(t_t)$ in Fig. 6, which is obtained by the modified Kibble-Zurek condition

$$\frac{1}{\Delta} = \frac{\|\hat{\mathrm{H}}_{\mathrm{TFI}}\|_\infty}{\|\partial_t \hat{\mathrm{H}}_{\mathrm{TFI}}\|_\infty}. \quad (42)$$

Explicitly, we find

$$\frac{1}{|h(\tau)-1|} = \frac{[h(\tau)+1]\,\mathcal{E}\left(\frac{4h(\tau)}{[h(\tau)+1]^2}\right)}{\pi\,\partial_t h(t)|_{t=\tau}}, \quad (43)$$

which we solved numerically to get $\Delta\tau_2(t_t)$ (green dashed line in Fig. 6). Finally, we also plotted the impulse interval $\Delta\tau_{\mathrm{opt}}(t_t)$, found by minimizing the distance between the fully evolved state and the AIA with respect to $\Delta\tau$, where we set the impulse instants to $\tau_{\mathrm{opt},\pm} = t_f/2 \pm \Delta\tau/2$. The result is depicted in Fig. 6 by a solid purple. Similar to the Landau-Zener model, we find that in the limit of large t_f, the optimal impulse interval can become negative (Fig. 6 inset). Showing that for certain final times t_f, one can get a better approximation to the fully evolved state by adiabatically crossing the quantum criticality and evolve up to τ_+, then make the "impulse jump" back to τ_-, to finally go again through the quantum phase transition.

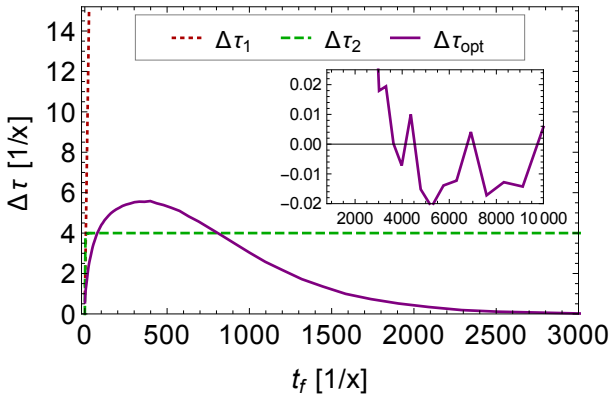

Figure 6. (Color online) A plot of the impulse interval $\Delta\tau_1(t_f)$ found by the Kibble-Zurek argument $1/\Delta = h/\partial_t h$, the impulse interval $\Delta\tau_2(t_t)$ given by the Kibble-Zurek argument using the inverse rate of change of the Hamiltonian $\frac{1}{\Delta} = \frac{\|\hat{\mathrm{H}}_{\mathrm{TFI}}\|_\infty}{\|\partial_t \hat{\mathrm{H}}_{\mathrm{TFI}}\|_\infty}$, and the optimal impulse interval $\Delta\tau_{\mathrm{opt}}(t_t)$ found by minimizing $\mathrm{d}_{\mathrm{aia}}$ with respect to $\Delta\tau$. The initial field was $h_i = 0.5$, the final $h_f = 1.5$ and the minimization was performed for a chain of $L = 150$.

The corresponding distances $\mathrm{d}_{\mathrm{adi}}$, $\mathrm{d}_{\mathrm{aia}-1}$, $\mathrm{d}_{\mathrm{aia}-2}$ and $\mathrm{d}_{\mathrm{aia}-\mathrm{opt}}$ are plotted as a function of t_f in Fig. 7, for the initial and final values $h_i = 0.5$, $h_f = 1.5$ and a chain with $L = 150$. We observe the following large t_f behavior, $\mathrm{d}_{\mathrm{adi}}(t_f) = 6.8\,t_f^{-1.07}$, $\mathrm{d}_{\mathrm{aia}-1}(t_f) = 20.3\,t_f^{-0.46}$, $\mathrm{d}_{\mathrm{aia}-2}(t_f) = 86.6\,t_f^{-1.00}$ and $\mathrm{d}_{\mathrm{aia}-\mathrm{opt}}(t_f) = 6.8\,t_f^{-1.07}$ (see gray lines in Fig. 7). The Kibble-Zurek argument gives an impulse interval that grows with $\sqrt{t_f}$, and thus the corresponding distance, $\mathrm{d}_{\mathrm{aia}-1}$, is always much larger than the adiabatic one. From this we conclude that $1/\Delta = \frac{h}{\partial_t h}$, clearly overestimates the impulse interval. However, we see $\mathrm{d}_{\mathrm{aia}-2} < \mathrm{d}_{\mathrm{adi}}$, up to $t_f = 10^3$, showing that the modified Kibble-Zurek argument yields a better estimate for the impulse interval. Although, for $t_f \geq 10^3$ we observe $\mathrm{d}_{\mathrm{adi}} \ll \mathrm{d}_{\mathrm{aia}-2}$, which implies that the impulse interval is still overestimated by the modified Kibble-Zurek argument. Obviously, the distance $\mathrm{d}_{\mathrm{aia}-\mathrm{opt}}$, where the impulse interval was found by minimizing the distance between the AIA and the full evolution, gives the smallest distance. Nevertheless, for our example of the transverse field Ising model the improvement compared to the simple adiabatic approximation is insignificant.

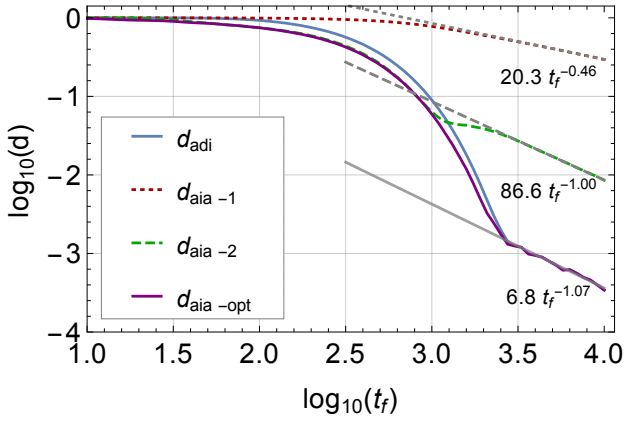

Figure 7. (Color online) The distance between the numerically evolved ground-state and the different approximation schemes, i.e., adiabatic, adiabatic-impulse with the Kibble-Zurek argument, with the modified Kibble-Zurek argument, and the adiabatic-impulse approximation where the impulse instants are found by minimization of $\mathrm{d}_{\mathrm{aia}}$, is shown for $h_i = 0.5$, $h_f = 1.5$ and $L = 150$.

III. ADIABATIC-IMPULSE APPROXIMATION IN OPEN SYSTEMS

In the following section we apply the AIA to the time evolution of open quantum systems. More specifically, we focus on dissipative systems characterized by a linear, time-local master equation in the Lindblad form. In a first step, we extend the AIA to the formalism used to describe open quantum system. To evaluate the accuracy of the AIA we will use the trace-norm distance between the fully evolved density matrix and the approximated one. We use the adiabatic approximation as a reference to asses the performance of the AIA. As an example,

we study the time evolution of a single qubit coupled to a thermal bath, where the Liouvillian is in the Davies form [41]. The Davies generators arise in the limit of weak system-bath coupling.

A. General setting

We consider an open quantum system of finite dimension, described by the density matrix $\hat{\rho}(t)$, whose evolution is governed by a linear and time-local master equation $\partial_t\hat{\rho} = \widehat{\mathcal{L}}(t)\hat{\rho}$. The Liouvillian $\widehat{\mathcal{L}}(t)$ is in the Lindblad form $\widehat{\mathcal{L}}(t)\hat{\rho} = -i\,[\hat{\mathrm{H}}(t),\hat{\rho}] + \sum_l[\hat{\mathrm{L}}_l(t)\hat{\rho}\hat{\mathrm{L}}_l^\dagger(t) - \frac{1}{2}\,\{\hat{\mathrm{L}}_l^\dagger(t)\hat{\mathrm{L}}_l(t),\hat{\rho}\}]$, where $\hat{\mathrm{H}}(t)$ is the system Hamiltonian and $\{\hat{\mathrm{L}}_l(t)\}$ are the Lindblad operators. Further, we assume that the time dependence enters through the parameter $\lambda(t)$. The instantaneous steady states are defined by $\widehat{\mathcal{L}}\hat{\rho}_1 = 0$, and belong to the kernel of the Liouvillian. We note that the Liouvillian operates on the space of linear operators acting on the Hilbert space, which is denoted by $\mathscr{L}(\mathcal{H})$. This space can be turned into a Hilbert space, when endowed with the Hilbert-Schmidt inner product $\langle\!\langle A|B\rangle\!\rangle = \mathrm{Tr}(\hat{\mathrm{A}}^\dagger\hat{\mathrm{B}})$, for $\hat{\mathrm{A}},\hat{\mathrm{B}} \in \mathscr{L}(\mathcal{H})$. We notice, that for a properly normalized basis of hermitian matrices $\{\hat{\Gamma}_j\}_{j=1}^{\dim\mathcal{H}^2}$, such that $\langle\!\langle\Gamma_i|\Gamma_j\rangle\!\rangle = \mathrm{Tr}(\hat{\Gamma}_i\hat{\Gamma}_j) = \delta_{ij}$, we can write the density matrix $\hat{\rho}$ as $|\rho\rangle\!\rangle = \sum_{k=1}^{\dim\mathcal{H}^2} c_k|\Gamma_k\rangle\!\rangle$, where $c_k = \langle\!\langle\Gamma_k|\rho\rangle\!\rangle = \mathrm{Tr}(\hat{\Gamma}_k\hat{\rho})$. The Liouvillian can therefore be interpreted as a matrix, $\widehat{\mathcal{L}} = \sum_{j,k=1}^{\dim\mathcal{H}^2}\mathcal{L}_{jk}|\Gamma_j\rangle\!\rangle\langle\!\langle\Gamma_k|$, with the coefficients given by $\mathcal{L}_{jk} = \langle\!\langle\Gamma_j|\widehat{\mathcal{L}}|\Gamma_k\rangle\!\rangle = \mathrm{Tr}[\hat{\Gamma}_j\widehat{\mathcal{L}}(\hat{\Gamma}_k)]$. In contrast to the Hamiltonian (closed systems) case, the eigenvalues of the Liouvillian can be complex numbers. We assume that the Liouvillian has only semisimple eigenvalues, i.e., has no Jordan blocks, or in terms of the corresponding projectors $\widehat{\mathcal{L}}(t)\widehat{P}_n(t) = l_n(t)\widehat{P}_n(t)$. This is guaranteed for the Davies generators, which we will consider in the example below, since then $\widehat{\mathcal{L}}$ is normal. The right and left eigenvectors of the Liouvillian are obtained by

$$\widehat{\mathcal{L}}|R_n^{(\alpha)}\rangle\!\rangle = l_n|R_n^{(\alpha)}\rangle\!\rangle, \quad \langle\!\langle L_m^{(\alpha)}|\widehat{\mathcal{L}} = l_m\langle\!\langle L_m^{(\alpha)}|, \tag{44}$$

where $n,m = 1,\ldots,\dim\mathcal{H}^2$ and α enumerates possible degeneracies. The right eigenvector $|R_1^\alpha\rangle\!\rangle$ of the eigenvalue $l_1 = 0$ are the instantaneous steady states in vector notation.

We will consider the protocol, where the system at $t = 0$ is initialized in the instantaneous steady state $\hat{\rho}_1(0)$, and then we tune the parameter $\lambda(t)$, from λ_i to $\lambda(t_f) = \lambda_f$, such that the gap of the Liouvillian becomes minimal at a single instant in time. The gap of the Liouvillian is defined as the minimum over all nonzero Lindbladian eigenvalues in absolute value.

Let us first recall the adiabatic approximation:

$$\hat{\rho}_{\mathrm{adi}}(t_f) = \widehat{U}(t_f,0)\hat{\rho}_1(0), \tag{45}$$

where $\widehat{U}(t_f,0)$ is the open system version of the full adiabatic intertwiner, i.e., the operator that adiabatically evolves all the levels, see Appendix B. Note that since $\hat{\rho}_1(0) \in \ker\widehat{\mathcal{L}}$, we have $\widehat{U}(t_f,0)\hat{\rho}_1(0) = \widehat{W}_1(t_f,0)\hat{\rho}_1(0)$, where $\widehat{W}_1(t_f,0)$ evolves adiabatically only vectors in the zero subspace (see Appendix A and [34] for more details).

Let us now consider the AIA. As in the closed case the evolution is assumed to be adiabatic from 0 to τ_-, then it suddenly jumps from τ_- to τ_+ (in the region where the Liouvillian/Hamiltonian gap is minimal), and finally becomes again adiabatic from τ_+ to t_f. Consequently, the AIA can be written as

$$\hat{\rho}_{\mathrm{aia}}(t_f) = \widehat{U}(t_f,\tau_+)\,\hat{1}\,\widehat{U}(\tau_-,0)\hat{\rho}_1(0). \tag{46}$$

At this point it is important to verify, whether the AIA map $\widehat{U}(t_f,\tau_+)\,\hat{1}\,\widehat{U}(\tau_-,0)$ is a bona fide completely positive trace preserving (CPTP) map. In the Appendix B we show that indeed the full intertwiner $\widehat{U}(t',t)$ is CPTP for $t' \geq t$, which in turn implies that the AIA map is CPTP. In doing so we actually prove an adiabatic theorem for the full intertwiner $\widehat{U}$. The whole complexity of the AIA lies in the determination of the adiabatic-impulse switching times $\tau_\pm$. For the Liouvillian in the Davies form we will simply use the Hamiltonian gap as the relevant energy scale.

To measure the closeness of the AIA and the adiabatic approximation to the time evolved state $\hat{\rho}(t_f)$, we use the trace-norm distance, which is defined by

$$\mathrm{d}(\hat{\rho},\hat{\sigma}) \equiv \frac{1}{2}\,\|\hat{\rho}-\hat{\sigma}\|_1 = \frac{1}{2}\sum_i s_i(\hat{\rho}-\hat{\sigma}), \tag{47}$$

where $s_i(\hat{\mathrm{X}})$ are the singular values of $\hat{\mathrm{X}}$. We note that for pure states the trace-norm distance reduces to the distance (9).

B. Single qubit coupled to a thermal bath

We will study a single qubit coupled to a thermal bath at inverse temperature $\beta = 1/T$. More specifically, the system Hamiltonian is assumed to be the Landau-Zener model, $\hat{\mathrm{H}}_{\mathrm{LZ}}(t) = x\hat{\sigma}^x + z(t)\hat{\sigma}^z$, whose gap is given by $\Delta(t) = 2\sqrt{x^2+z(t)^2}$. The system-bath interaction is characterized by $\hat{\mathrm{H}}_{\mathrm{int}} = g\,\hat{\sigma}^y\otimes\hat{\mathrm{B}}$, where g is the system-bath coupling constant, and $\hat{\mathrm{B}}$ some bath operator. $\hat{\mathrm{H}}_{\mathrm{b}}$ describes the Hamiltonian of the bath. Consequently, the total Hamiltonian reads $\hat{\mathrm{H}}_{\mathrm{tot}}(t) = \hat{\mathrm{H}}_{\mathrm{LZ}}(t)+\hat{\mathrm{H}}_{\mathrm{int}}+\hat{\mathrm{H}}_{\mathrm{b}}$. We use a weak system-bath coupling and a slowly varying system Hamiltonian [42], therefore the time-dependent Lindblad master-equation approximation describing the dynamics of the density matrix $\hat{\rho}(t)$, is assumed to be in the Davies form [41],

$$\widehat{\mathcal{L}}(t)\hat{\rho} = -i\,[\hat{\mathrm{H}}_{\mathrm{LZ}}(t),\hat{\rho}] + \sum_{\omega=\{0,\pm\Delta\}}\gamma(\omega)[\hat{\mathrm{L}}_\omega(t)\,\hat{\rho}\,\hat{\mathrm{L}}_\omega^\dagger(t) - \frac{1}{2}\,\{\hat{\mathrm{L}}_\omega^\dagger(t)\,\hat{\mathrm{L}}_\omega(t),\hat{\rho}\}], \tag{48}$$

where the spectral function of the bath $\gamma(\omega)$ is positive and satisfies the Kubo-Martin-Schwinger (KMS) condition $\gamma(-\omega) = e^{-\beta\omega}\gamma(\omega)$, see Ref. [43]. Let us choose $\gamma(\omega)$ to be in the Ohmic form

$$\gamma(\omega) = 2\pi g^2 \frac{\omega}{1 - e^{-\beta\omega}}. \tag{49}$$

We note that the Davis form guarantees the steady states to be of the Gibbs form, $\hat{\rho}_1 = e^{-\beta \hat{\mathrm{H}}_{\mathrm{LZ}}}/Z$, with $Z = \mathrm{Tr}_S(e^{-\beta \hat{\mathrm{H}}_{\mathrm{LZ}}})$, see [44] for more details. The choice of $\hat{\mathrm{H}}_{\mathrm{int}} = g\,\hat{\sigma}^y \otimes \hat{\mathrm{B}}$, ensure the minimum Lindbladian gap to be nonzero for all z, thus we have as in the Landau-Zener case an avoided level crossing. Further, we note that the Lamb shift Hamiltonian was neglected for simplicity. Finally, the Lindblad operators are given by

$$\hat{\mathrm{L}}_\omega(t) = \sum_{i,j:\ E_i - E_j = \omega} |\psi_i\rangle\langle\psi_i|\hat{\sigma}^y|\psi_j\rangle\langle\psi_j|, \tag{50}$$

where $\omega \in \{0, \pm\Delta\}$, $i, j \in \{1, 2\}$, $E_{1,2} = \pm\sqrt{x^2 + z^2}$ are the eigenenergies of the Landau-Zener model and $|\psi_i\rangle$ denote the corresponding eigenstates given in Eq. (11), and we obtain

$$\hat{\mathrm{L}}_0 = 0, \quad \hat{\mathrm{L}}_{+\Delta} = \frac{i\,z}{2\,b}\hat{\sigma}^x + \frac{1}{2}\hat{\sigma}^y - \frac{i\,x}{2\,b}\hat{\sigma}^z = (\hat{\mathrm{L}}_{-\Delta})^\dagger. \tag{51}$$

The eigenvalues of the resulting Liouvillian $\widehat{\mathcal{L}}(t)$ are given by

$$l_1 = 0, \tag{52}$$

$$l_2 = -\left[\gamma(-\Delta) + \gamma(\Delta)\right] = -2\pi g^2 \Delta \coth(\frac{\beta\Delta}{2}), \tag{53}$$

$$l_3 = \frac{\lambda_2}{2} - i\Delta = -\pi g^2 \Delta \coth(\frac{\beta\Delta}{2}) - i\Delta, \tag{54}$$

$$l_4 = \frac{\lambda_2}{2} + i\Delta = -\pi g^2 \Delta \coth(\frac{\beta\Delta}{2}) + i\Delta, \tag{55}$$

which are derived in Appendix C. The corresponding left and right eigenvectors, denoted by $\langle\langle L_i|$ and $|R_i\rangle\rangle$, respectively, with $i = 1, 2, 3, 4$, are also given in Appendix C.

As for the closed case, we assume the protocol, where x is constant in time, $z(t) = z_i + (z_f - z_i)\,t/t_f$, with $t \in [0, t_f]$, and the system prepared in the state $\hat{\rho}(0) = \hat{\rho}_1(0)$. For the initial point, z_i, we choose a negative value, and for the final point, z_f, the same but positive value, such that the protocol passes the avoided level crossing (minimal gap) at $z = 0$. The time evolution is described by a linear, time-local master equation of the form $\partial_t\hat{\rho} = \widehat{\mathcal{L}}(t)\hat{\rho}$, which we express in the basis $\frac{1}{\sqrt{2}}\{\hat{1}, \hat{\sigma}^x, \hat{\sigma}^y, \hat{\sigma}^z\}$ and solve numerically (see Appendix D).

First, we study the adiabatic approximation of the time evolved state, $\hat{\rho}(t_f)$, given by

$$\hat{\rho}_{\mathrm{adi}}(t_f) = \widehat{U}(t_f, 0)\hat{\rho}_1(0). \tag{56}$$

Note that since $\hat{\rho}_1(0) \in \ker\widehat{\mathcal{L}}$ and the latter is one dimensional, we have

$$|\rho_{\mathrm{adi}}(t_f)\rangle\rangle = |R_1(t_f)\rangle\rangle. \tag{57}$$

The dynamical phase is zero, since $l_1 = 0$, and the Berry phase is also zero, due to the fact that $\langle\langle L_j|\partial_z|R_j\rangle\rangle = 0$, for $j = 1, 2, 3, 4$.

Within the AIA the time evolved state of our system is approximated by

$$\hat{\rho}_{\mathrm{aia}}(t_f) = \widehat{U}(t_f, \tau_+)\,\hat{1}\,\widehat{U}(\tau_-, 0)\hat{\rho}_1(0). \tag{58}$$

In vector notation we find

$$|\rho_{\mathrm{aia}}(t_f)\rangle\rangle = \sum_{j=1}^{4} e^{\ell_j(\tau_+, t_f)}\langle\langle L_j(\tau_+)|\,R_1(\tau_-)\rangle\rangle|R_j(t_f)\rangle\rangle, \tag{59}$$

where the dynamical phase reads, $\ell_j(\tau_+, t_f) = \int_{\tau_+}^{t_f} dt\, l_j$, and the Berry phases vanish as mentioned above. To estimate the adiabatic-impulse switching times, $\tau_\pm$, we will use the gap Δ of the system Hamiltonian, and therefore refer to the Sec. II B for the estimation of $\tau_\pm$.

The trace-norm distance between the exact evolution and the adiabatic approximation/AIA are shown in Fig. 8 for different temperatures T, and for $x = 0.1$, $z_i = -1$, $z_f = 1$ and $g = 0.01$. In Fig. 8 (a) we plot $\mathrm{d}_{\mathrm{adi}}(t_f)$ and in Fig. 8 (b) $\mathrm{d}_{\mathrm{aia}-1}(t_f)$, where the impulse interval was estimated by the Kibble-Zurek argument using the gap Δ of $\hat{\mathrm{H}}_{\mathrm{LZ}}$, i.e., $1/\Delta = z/\partial_t z$. As in the closed case, we find that the AIA performs only better than the adiabatic approximation for short times $t_f < 10^2$. However, for intermediate times, $10^2 < t_f < 10^4$, the AIA is considerably worse than the adiabatic approximation. In contrast to the closed case, we observe that the trace-norm distance $\mathrm{d}_{\mathrm{adi}}(t_f)$ and $\mathrm{d}_{\mathrm{aia}-1}(t_f)$ become the same for large t_f. We believe an important ingredient to understand this phenomena is the fact that the $\ker(\widehat{\mathcal{L}})$ is one-dimensional.

In Fig. 9 (a) we plot the impulse interval $\Delta\tau_1$ obtained by the Kibble-Zurek argument $1/\Delta = z/\partial_t z$, $\Delta\tau_2$ given by the modified Kibble-Zurek argument $1/\Delta = \|\hat{\mathrm{H}}_{\mathrm{LZ}}\| \,/\, \|\partial_t \hat{\mathrm{H}}_{\mathrm{LZ}}\|$, and $\Delta\tau_{\mathrm{opt}}$ found by minimizing the trace-norm distance $\mathrm{d}_{\mathrm{aia}}$ with respect to $\Delta\tau$. The resulting trace-norm distances are compared in Fig. 9 (b). It is interesting to see that for large t_f all the approximation schemes give the same trace norm distance as the adiabatic approximation. We observe although, that the first order adiabatic correction still provides a smaller distance. Even the trace norm distance found by the minimization process becomes the same as the simple adiabatic approximation. We note that the first order correction to the adiabatic approximation can be found in Ref. [35] (Theorem 6). However, there is a regime for which $\mathrm{d}_{\mathrm{opt}}$ can reach the same distance as the first order adiabatic approximation, if the counter intuitive scheme of crossing the minimal gap region twice is applied.

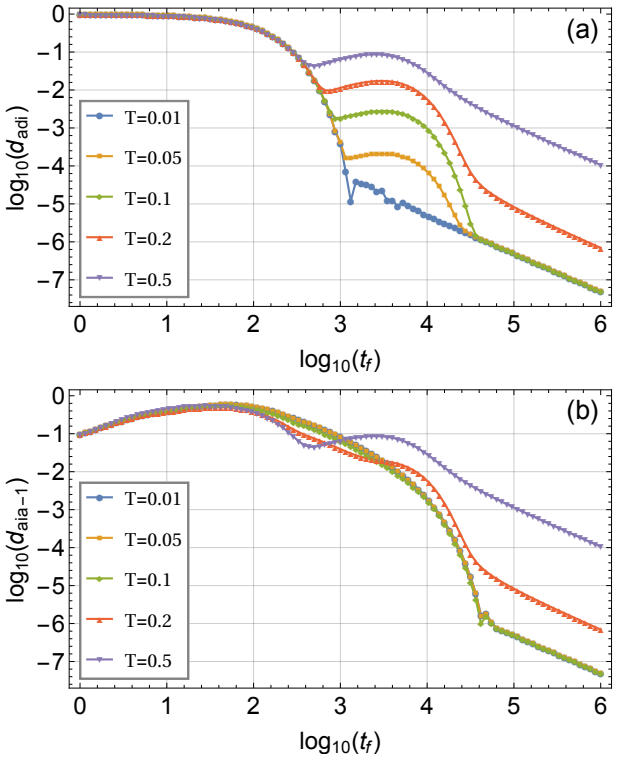

Figure 8. (Color online) The trace-norm distance between the fully evolved state and the adiabatic/adiabatic-impulse approximation is shown. The impulse interval for the adiabatic-impulse approximation was obtained by the Kibble-Zurek argument $1/\Delta = z/\partial_t z$. The panel (a) shows $\mathrm{d_{adi}}(t_f)$ and the panel (b) depicts $\mathrm{d_{aia-1}}(t_f)$ on a logarithmic scale. We plotted the trace-norm distance for different temperatures and for $x = 0.1$, $z_i = -1$, $z_f = 1$, and $g = 0.01$.

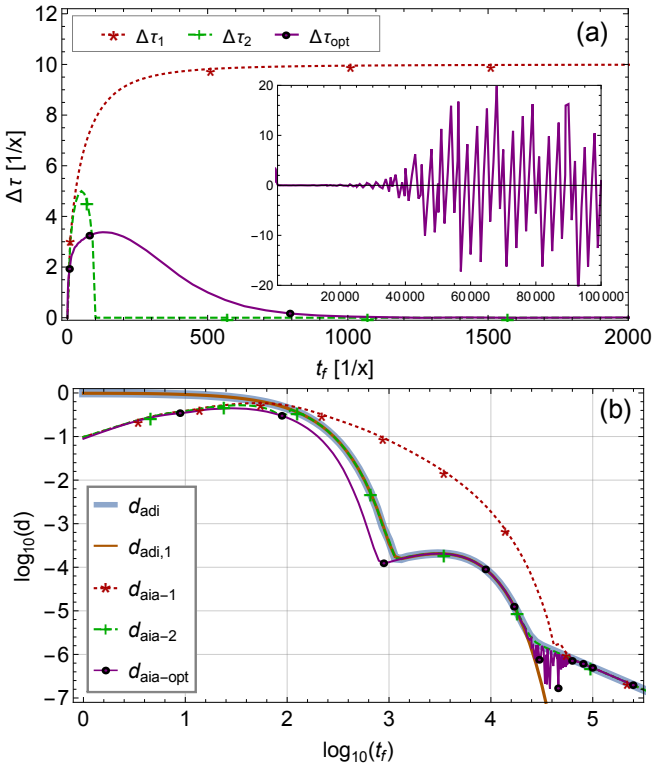

Figure 9. (Color online) (a) We plot the impulse interval $\Delta\tau_1$ obtained by the Kibble-Zurek argument $1/\Delta = z/\partial_t z$, $\Delta\tau_2$ determined by the Kibble-Zurek argument using the rate of change of the Hamiltonian $1/\Delta = \|\hat{\mathrm{H}}_{\mathrm{LZ}}\| \,/\, \|\partial_t \hat{\mathrm{H}}_{\mathrm{LZ}}\|$, and the optimal impulse interval $\Delta\tau_{\mathrm{opt}}$ found by minimizing the trace-norm distance $\mathrm{d_{aia}}$ with respect to $\Delta\tau$. (b) We compare the trace-norm distance found by the different scenarios mentioned in (a). The following values were used in both panels $T = 0.05$, $x = 0.1$, $z_i = -1$, $z_f = 1$, and $g = 0.01$.

IV. CONCLUSIONS

We studied the accuracy of the AIA for closed and open quantum systems, by evaluating how well this approximation reproduces the exactly evolved state of the system. We used the trace-norm distance to characterize the closeness of the approximated state to the exactly evolved one. The adiabatic approximation served as a reference for the evaluation of the AIA. As might be expected, the AIA performs better than the adiabatic approximation for small total evolution times t_f. For large total evolution times, we observed that the Kibble-Zurek argument overestimates the impulse interval and thus the AIA provided a poor approximation to the time evolved state.

Modifying the Kibble-Zurek argument allowed us to improve the AIA, such that at least the adiabatic approximation can be recovered. However, the AIA can outperform the adiabatic one for large t_f, if a counter intuitive procedure is applied. Namely, driving the system adiabatically through the region where the gap is minimal, then jumping back, to cross the minimal gap region once again adiabatically. We illustrated by several examples, that it is highly non trivial to estimate the optimal impulse regime and even harder to guess, when to cross the minimal gap twice, using this counter intuitive recipe.

We conclude, that the adiabatic-impulse approximation is a good method to estimate the scaling behavior of certain non-equilibrium properties, see, e.g., [14–16] for closed quantum systems or for dissipative quantum systems [45–48]. Nevertheless, to use it as a rigorous approximation for the time evolution of quantum systems that are driven across a minimal gap region, one still needs to get nontrivial knowledge about the system's properties.

V. ACKNOWLEDGMENTS

The research is based upon work (partially) supported by the Office of the Director of National Intelligence (ODNI), Intelligence Advanced Research Projects Activity (IARPA), via the U.S. Army Research Office contract W911NF-17-C-0050. The views and conclusions contained herein are those of the authors and should not be interpreted as necessarily representing the official policies or endorsements, either expressed or implied, of the ODNI, IARPA, or the U.S. Government. The U.S. Government is authorized to reproduce and distribute reprints for Governmental purposes notwithstanding any copyright annotation thereon. This work was also supported by the Swiss National Science Foundation (SNSF) and by the ARO MURI grant W911NF-11-1-0268. M.T. is grateful to R. Di Felice and the CNR-NANO Institute in Modena, Italy for their kind hospitality. M.T. would also like to thank G. Styliaris and J. Marshall for helpful discussions.

Appendix A: Adiabatic intertwiner for a single level

In this appendix we express the adiabatic intertwiner $\widehat{W}_1(t_2,t_1)$, which evolves adiabatically a single instantaneous steady state of the Liouvillian from t_1 to t_2, in vector notation. In case the evolution is a long a closed loop the adiabatic intertwiner becomes the so called Wilczek-Zee operator [49, 50]. The instantaneous steady states, i.e., the states from the kernel of the Liouvillian $\widehat{\mathcal{L}}(t)$, are defined by $\widehat{\mathcal{L}}(t)\hat{\rho}_1^{(\alpha)}(t)=0$, where α enumerates possible degeneracy. In vector notation the instantaneous steady states $\hat{\rho}_1^{(\alpha)}(t)$ are the right eigenvectors of the Liouvillian given by $\widehat{\mathcal{L}}(t)|R_1^{(\alpha)}\rangle\!\rangle=0$. Further, the instantaneous spectral projection of $\widehat{\mathcal{L}}(t)$ with zero eigenvalue is denoted by $\widehat{P}_1(t)$. We note that for a Liouvillian in the Lindblad form, the zero eigenvalue (possibly degenerate) is semisimple, i.e., there are no Jordan blocks associated to the zero eigenvalue and thus there are no nilpotent terms in the zero sector, $\widehat{\mathcal{L}}\widehat{P}_1=\widehat{P}_1\widehat{\mathcal{L}}=0$, see [34] for a detailed proof.

The ideal adiabatic evolution is described by an operator $\widehat{V}_1(t,0)$, satisfying the intertwining property $\widehat{V}_1(t,0)\widehat{P}_1(0)=\widehat{P}_1(t)\widehat{V}_1(t,0)$ and is given by the solution of

$$\partial_t\widehat{V}_1(t,0)=[\partial_t\widehat{P}_1(t),\widehat{P}_1(t)]\,\widehat{V}_1(t,0) \tag{A1}$$

$$\widehat{V}_1(0,0)=\hat{1}, \tag{A2}$$

where $\hat{1}$ is the identity operator. One can see that $\widehat{V}_1(t,0)$ is not, in general, a completely positive trace preserving (CPTP) map [34], however $\widehat{W}_1(t,0)\equiv\widehat{V}_1(t,0)\widehat{P}_1(0)$ is a CPTP map and thus the proper adiabatic intertwiner, i.e., $\hat{\rho}_1^{(\alpha)}(t)=\widehat{W}_1(t,0)\hat{\rho}_1^{(\alpha)}(0)$. In addition, it was shown in [34], that we can write

$$\widehat{W}_1(t,0)=\lim_{N\to\infty}\widehat{P}_1(N\epsilon)\cdots\widehat{P}_1(2\epsilon)\widehat{P}_1(\epsilon)\widehat{P}_1(0). \tag{A3}$$

where $(t=N\epsilon)$. So we write

$$\widehat{P}_1(t)=\sum_\alpha|R_1^{(\alpha)}(t)\rangle\!\rangle\langle\!\langle L_1^{(\alpha)}(t)|, \tag{A4}$$

and note that

$$\begin{aligned}
&\langle\!\langle L_1^{(\alpha_{j+1})}(t_{j+1})|R_1^{(\alpha_j)}(t_j)\rangle\!\rangle\\
&=\delta_{\alpha_{j+1},\alpha_j}+\epsilon\,\langle\!\langle L_1^{(\alpha_{j+1})}(t)|\overleftarrow{\partial}_t|_{t=t_j}|R_1^{(\alpha_j)}(t_j)\rangle\!\rangle+O\left(\epsilon^2\right)\\
&=\delta_{\alpha_{j+1},\alpha_j}-\epsilon\,\langle\!\langle L_1^{(\alpha_{j+1})}(t_j)|\partial_t|R_1^{(\alpha_j)}(t)\rangle\!\rangle|_{t=t_j}+O\left(\epsilon^2\right)\\
&=[\mathbb{1}-\epsilon A(t_j)]_{\alpha_{j+1},\alpha_j}+O\left(\epsilon^2\right),
\end{aligned} \tag{A5}$$

where $t_j=\epsilon j$, with $j=0,1,\ldots,N$ and $t_N=t$. The second line follows by differentiating $\langle\!\langle L_1^{(\alpha)}|R_1^{(\beta)}\rangle\!\rangle=\delta_{\alpha,\beta}$ and we defined $[A_1(t)]_{\alpha,\beta}\equiv\langle\!\langle L_1^{(\alpha)}(t)|\partial_t|R_1^{(\beta)}(t)\rangle\!\rangle$. Plug-

ging Eq. (A5) into Eq. (A3) yields

$$\widehat{W}_1(t,0) = \sum_{\alpha_N,\alpha_0} |R_1^{(\alpha_N)}(t)\rangle\!\rangle\langle\!\langle L_1^{(\alpha_0)}(0)| \left[\overleftarrow{\mathrm{T}}\mathrm{exp}\left[-\int_0^t A_1(\sigma)d\sigma\right]\right]_{\alpha_N,\alpha_0}, \quad \text{(A6)}$$

where $\overleftarrow{\mathrm{T}}$ is the so called time-ordering operator, ordering the operators in a chronological order with time increasing from right to left. Now we note further that,

$$\left\{\overleftarrow{\mathrm{T}}\mathrm{exp}\left[-\int_0^t A_1(\sigma)d\sigma\right]\right\}^T = \overrightarrow{\mathrm{T}}\mathrm{exp}\left[-\int_0^t A_1^T(\sigma)d\sigma\right], \quad \text{(A7)}$$

where T indicates transpose and $\overrightarrow{\mathrm{T}}$ arranges operators in a chronological order, with time increasing from left to right. Finally, we can write

$$\widehat{W}_1(t,0) = \sum_{\alpha_N,\alpha_0} |R_1^{(\alpha_N)}(t)\rangle\!\rangle\langle\!\langle L_1^{(\alpha_0)}(0)| \cdot \left[\overrightarrow{\mathrm{T}}\mathrm{exp}\left[-\int_0^t A^T(\sigma)d\sigma\right]\right]_{\alpha_0,\alpha_N}, \quad \text{(A8)}$$

which is the formula usually found in the literature [49, 50].

Appendix B: The full adiabatic intertwiner

In this appendix we want to show that the full adiabatic intertwiner $\widehat{U}$, i.e., the map that evolves adiabatically all the levels and not only a single one, is a bona fide completely positive trace preserving (CPTP) map. In doing so we will also prove the adiabatic theorem for $\widehat{U}$. First, we note that it is convenient to rescale the time by the total evolution time t_f, $s(t) = t/t_f$, such that $s \in [0,1]$. Second, we remark that the dot will stand for differentiation with respect to s, $\dot{X} = \partial_s X$. Further, we assume the following spectral resolution of the Liouvillian $\widehat{\mathcal{L}}(s)\widehat{P}_n(s) = l_n(s)\widehat{P}_n(s)$, in other words we assume no Jordan blocks. We also assume that all the levels $l_n(s)$ do not cross and $\widehat{P}_n(s)$ are twice differentiable.

We begin by defining $V_n(s,s')$ as the solution of the following ODE

$$\dot{\widehat{V}}_n = \left(t_f\widehat{\mathcal{L}} + [\dot{\widehat{P}}_n, \widehat{P}_n]\right)\widehat{V}_n, \quad \widehat{V}_n(0) = \hat{1}. \quad \text{(B1)}$$

Differentiating $\widehat{h}(s,s') \equiv \widehat{V}_n(s,s')\widehat{P}_n(s')\widehat{V}_n(s',0)$ with respect to s', one sees that $\widehat{V}_n(s)$ has the intertwining property:

$$\widehat{P}_n(s)\widehat{V}_n(s) = \widehat{V}_n(s)\widehat{P}_n(0). \quad \text{(B2)}$$

Let us define also $\widehat{W}_n(s) \equiv \widehat{P}_n(s)\widehat{V}_n(s)$. Using $\dot{\widehat{P}}_n = \widehat{P}_n\dot{\widehat{P}}_n + \dot{\widehat{P}}_n\widehat{P}_n$, one realizes that

$$\dot{\widehat{W}}_n = (t_f\widehat{\mathcal{L}} + \dot{\widehat{P}}_n)\widehat{W}_n = \left(t_f\widehat{\mathcal{L}} + [\dot{\widehat{P}}_n, \widehat{P}_n]\right)\widehat{W}_n. \quad \text{(B3)}$$

Since $\widehat{W}_n$ satisfies the same ODE as $\widehat{V}_n$, but with a different initial condition, we see that $\widehat{W}_n$ satisfies the intertwining property.

Let us now further define

$$\widehat{U}(s) \equiv \sum_n \widehat{W}_n(s). \quad \text{(B4)}$$

We note that we assumed $\sum_n \widehat{P}_n = \hat{1}$, i.e., that the eigenvectors span the full space. If this is not the case, i.e., there is also a continuous spectrum, one can use the trick due to Kato, defining the "missing" $\widehat{P}_0(s)$, such that the $\widehat{P}_n$ are then complete. The differential equation for $\widehat{U}$ is

$$\dot{\widehat{U}} = \sum_n (t_f\widehat{\mathcal{L}}\widehat{P}_n + \dot{\widehat{P}}_n\widehat{P}_n)\widehat{W}_n = \sum_n (t_f\widehat{\mathcal{L}}\widehat{P}_n + \dot{\widehat{P}}_n\widehat{P}_n)\sum_l \widehat{W}_l. \quad \text{(B5)}$$

Now using $\sum_n \dot{\widehat{P}}_n\widehat{P}_n = -\sum_n \widehat{P}_n\dot{\widehat{P}}_n$, which stems from the completeness of the $\widehat{P}_n$, one gets

$$\dot{\widehat{U}} = \left(t_f\widehat{\mathcal{L}} + \frac{1}{2}\sum_n [\dot{\widehat{P}}_n, \widehat{P}_n]\right)\widehat{U}, \quad \widehat{U}(0) = \sum_n \widehat{P}_n(0) = \hat{1}. \quad \text{(B6)}$$

Clearly, $\widehat{U}(s)$ behaves like $\widehat{W}_n(s)$ in the range of $\widehat{P}_n(0)$ for all n, so $\widehat{U}(s)$ might as well be called the full intertwiner.

Let us now show that each $\widehat{V}_n$ is close to $\widehat{\mathcal{E}}$ in the range of $\widehat{P}_n$, where the operator $\widehat{\mathcal{E}}(s,0)$ is the evolution operator, describing the full time evolution of the density matrix $\hat{\rho}(s) = \widehat{\mathcal{E}}(s,0)\hat{\rho}(0)$, and satisfies $\partial_s\widehat{\mathcal{E}}(s,0) = t_f\widehat{\mathcal{L}}(s)\widehat{\mathcal{E}}(s,0)$, with $\widehat{\mathcal{E}}(s,s) = \hat{1}$. One has

$$\begin{aligned}\widehat{\mathcal{E}}(0,s)\widehat{W}_n(s) - \widehat{P}_n(0) &= \int_0^s ds' \frac{d}{ds'}\left[\widehat{\mathcal{E}}(0,s')\widehat{W}_n(s')\right] \\ &= \int_0^s ds'\widehat{\mathcal{E}}(0,s')\dot{\widehat{P}}_n(s')\widehat{W}_n(s') \\ &= \int_0^s ds'\widehat{\mathcal{E}}(0,s')\widehat{Q}_n(s')\dot{\widehat{P}}_n(s')\widehat{W}_n(s'), \end{aligned} \quad \text{(B7)}$$

where $\widehat{Q}_n(s) = \hat{1} - \widehat{P}_n(s)$, and by using the identity $\widehat{P}_n\dot{\widehat{P}}_n\widehat{P}_n = 0$. The reduced resolvent is defined by $\widehat{S}_n = \lim_{a\to l_n}\widehat{Q}_n(\widehat{\mathcal{L}} - a\hat{1})^{-1}\widehat{Q}_n$, which satisfies $\widehat{Q}_n = \widehat{\mathcal{L}}\widehat{S}_n$, and together with

$$\widehat{\mathcal{E}}(0,s')\widehat{\mathcal{L}}(s') = -t_f^{-1}\partial_{s'}\widehat{\mathcal{E}}(0,s'), \quad \text{(B8)}$$

implies

$$\begin{aligned}
&\widehat{\mathcal{E}}(0,s)\widehat{W}_n(s) - \widehat{P}_n(0) \\
&= -\frac{1}{t_f}\int_0^s ds' \left[\partial_{s'}\widehat{\mathcal{E}}(0,s')\right] \widehat{S}_n(s')\dot{\widehat{P}}_n(s')\widehat{W}_n(s') \\
&= -\frac{1}{t_f}\,\widehat{\mathcal{E}}(0,s')\widehat{S}_n(s')\dot{\widehat{P}}_n(s')\widehat{W}_n(s')\Big|_0^s \\
&+ \frac{1}{t_f}\int_0^s ds'\widehat{\mathcal{E}}(0,s')\partial_{s'}\left[\widehat{S}_n(s')\dot{\widehat{P}}_n(s')\widehat{W}_n(s')\right]. \qquad \text{(B9)}
\end{aligned}$$

We now multiply the last equation by $\widehat{\mathcal{E}}(s,0)$ from the left and get

$$\begin{aligned}
&\widehat{\mathcal{E}}(s,0)\widehat{P}_n(0) - \widehat{V}_n(s)\widehat{P}_n(0) \\
&= \frac{1}{t_f}\left[\widehat{S}_n(s)\dot{\widehat{P}}_n(s)\widehat{W}_n(s) - \widehat{\mathcal{E}}(s,0)\widehat{S}_n(0)\dot{\widehat{P}}_n(0)\widehat{W}_n(0)\right] \\
&- \frac{1}{t_f}\int_0^s ds'\widehat{\mathcal{E}}(s,s')\partial_{s'}\left[\widehat{S}_n(s')\dot{\widehat{P}}_n(s')\widehat{W}_n(s')\right]. \qquad \text{(B10)}
\end{aligned}$$

We note that $\widehat{S}_n$ is the reduced resolvent of $\widehat{\mathcal{L}}$ and does not contain t_f, so neither $\widehat{S}_n$ nor $\widehat{P}_n$ depend on t_f. However, in our formulation $\widehat{W}_n$ does depend on t_f. In [51] Salem simply claims that $\widehat{W}_n$ is bounded. This seems to overlook the fact that the constant for the bound could still depend on t_f. In any case, the required bound can be obtained by writing a Trotter expansion for $\widehat{W}_n$:

$$\widehat{W}_n(s) = \lim_{N\to\infty} \overleftarrow{\mathrm{T}} \prod_{i=1}^{N}\left(e^{\epsilon t_f \widehat{\mathcal{L}}(s_i)} e^{\epsilon \dot{\widehat{P}}_n(s_i)}\right) \qquad \text{(B11)}$$

with $\epsilon = s/N$, $s_i = \epsilon i$. This shows that $\|\widehat{W}_n\|$ can be bounded by a constant independent of t_f, since each $\widehat{\mathcal{L}}$ is a generator of a contraction semigroup. In fact one obtains

$$\left\|\widehat{W}_n(s)\right\| \le \exp\left(\int_0^s ds' \left\|\dot{\widehat{P}}_n(s')\right\|\right), \qquad \text{(B12)}$$

which shows finally that

$$\left\|\left(\widehat{\mathcal{E}}(s) - \widehat{W}_n(s)\right)\widehat{P}_n(0)\right\| \le \frac{C_n}{t_f}, \qquad \text{(B13)}$$

where C_n are finite constants independent of t_f. Coming back to $\widehat{U}$, we can write

$$\begin{aligned}
\widehat{\mathcal{E}}(s) - \widehat{U}(s) &= \sum_n \left[\widehat{\mathcal{E}}(s) - \widehat{U}(s)\right]\widehat{P}_n(0) \\
&= \sum_n \left[\widehat{\mathcal{E}}(s) - \widehat{W}_n(s)\right]\widehat{P}_n(0), \qquad \text{(B14)}
\end{aligned}$$

and taking the norm one obtains

$$\left\|\widehat{\mathcal{E}}(s) - \widehat{U}(s)\right\| \le \frac{1}{t_f}\sum_n C_n. \qquad \text{(B15)}$$

In finite dimension the latter sum $\sum_n C_n$ does not pose a problem, since it is still finite. Nevertheless, for infinite dimensional systems one should show that the sum is bounded. In summary, this implies that $\widehat{U}$ is arbitrarily close to a CPTP map, and therefore is itself a CPTP map.

Appendix C: Derivation of the eigenvalues and eigenvectors of the Liouvillian

Let us now write the Liouvillian operator $\widehat{\mathcal{L}}$ in the basis $\{\hat{\Gamma}_i\}_{i=1}^4 = \frac{1}{\sqrt{2}}\{\hat{1}, \hat{\sigma}^x, \hat{\sigma}^y, \hat{\sigma}^z\}$, i.e., $\mathcal{L}_{ij} = \mathrm{Tr}(\hat{\Gamma}_i\,\widehat{\mathcal{L}}\,\hat{\Gamma}_j)$, we find

$$(\mathcal{L}_{ij}) = \begin{pmatrix}
0 & 0 & 0 & 0 \\
\frac{2x}{\Delta}\left[\gamma(-\Delta) - \gamma(\Delta)\right] & -\frac{2(x^2 + \frac{1}{4}\Delta^2)\left[\gamma(-\Delta) + \gamma(\Delta)\right]}{\Delta^2} & -2z & -\frac{2xz\left[\gamma(-\Delta) + \gamma(\Delta)\right]}{\Delta^2} \\
0 & 2z & -\frac{1}{2}\left[\gamma(-\Delta) - \gamma(\Delta)\right] & -2x \\
\frac{2z\left[\gamma(-\Delta) - \gamma(\Delta)\right]}{\Delta} & -\frac{2xz\left[\gamma(-\Delta) + \gamma(\Delta)\right]}{\Delta^2} & 2x & -\frac{2(\frac{1}{4}\Delta^2 + z^2)\left[\gamma(-\Delta) + \gamma(\Delta)\right]}{\Delta^2}
\end{pmatrix}, \qquad \text{(C1)}$$

and the vector representation of the density matrix $\hat{\rho}$ reads

$$|\rho\rangle\!\rangle = \sum_{i=1}^{4} c_i |\Gamma_i\rangle\!\rangle = \begin{pmatrix} c_1 \\ c_2 \\ c_3 \\ c_4 \end{pmatrix}, \qquad \text{(C2)}$$

where $c_i = \mathrm{Tr}(\hat{\Gamma}_i\hat{\rho})$. The eigenvalues of the Liouvillian $\mathcal{L}$ can be calculated and are given by

$$l_1 = 0, \qquad \text{(C3)}$$

$$l_2 = -\left[\gamma(-\Delta) + \gamma(\Delta)\right] = -2\pi g^2 \Delta \coth(\frac{\Delta}{2}\beta), \qquad \text{(C4)}$$

$$l_3 = -\frac{1}{2}\left[\gamma(-\Delta) + \gamma(\Delta)\right] - i\Delta = -\pi g^2 \Delta \coth(\frac{\Delta}{2}\beta) - i\Delta, \qquad \text{(C5)}$$

$$l_4 = -\frac{1}{2}\left[\gamma(-\Delta) + \gamma(\Delta)\right] + i\Delta = -\pi g^2 \Delta \coth(\frac{\Delta}{2}\beta) + i\Delta, \qquad \text{(C6)}$$

and the corresponding eigenvectors read

$$|r_1\rangle\!\rangle = \begin{pmatrix} \frac{\Delta}{\sqrt{2}\,z}\frac{\gamma(-\Delta)+\gamma(\Delta)}{\gamma(-\Delta)-\gamma(\Delta)} \\ \frac{x}{z} \\ 0 \\ 1 \end{pmatrix} = \begin{pmatrix} -\frac{\Delta}{\sqrt{2}\,z}\coth(\frac{\beta\Delta}{2}) \\ \frac{x}{z} \\ 0 \\ 1 \end{pmatrix},$$

$$|r_2\rangle\!\rangle = \begin{pmatrix} 0 \\ \frac{x}{z} \\ 0 \\ 1 \end{pmatrix}, \quad |r_3\rangle\!\rangle = \begin{pmatrix} 0 \\ -\frac{z}{x} \\ -i\frac{\Delta}{2\,x} \\ 1 \end{pmatrix}, \quad |r_4\rangle\!\rangle = \begin{pmatrix} 0 \\ -\frac{z}{x} \\ i\frac{\Delta}{2\,x} \\ 1 \end{pmatrix}. \tag{C7}$$

We note that they have to be normalized such that the corresponding density matrices have trace one. Since $\hat{\rho} = \sum_i c_i \hat{\Gamma}_i = c_1\frac{1}{\sqrt{2}}\hat{1} + c_2\frac{1}{\sqrt{2}}\hat{\sigma}^x + c_3\frac{1}{\sqrt{2}}\hat{\sigma}^y + c_4\frac{1}{\sqrt{2}}\hat{\sigma}^z$, only the first component needs to be $\frac{1}{\sqrt{2}}$ in order to have $\mathrm{Tr}(\hat{\rho}) = 1$, because $\mathrm{Tr}(\hat{1}) = 2$ and $\mathrm{Tr}(\hat{\sigma}^\alpha) = 0$ for $\alpha = x, y, z$. As we see this is only possible for the right eigenvector $|r_1\rangle\!\rangle$ with $l_1 = 0$, and therefore we find

$$|\rho_1\rangle\!\rangle = \begin{pmatrix} \frac{1}{\sqrt{2}} \\ -\frac{\sqrt{2}x}{\Delta}\tanh(\frac{\beta\Delta}{2}) \\ 0 \\ -\frac{\sqrt{2}z}{\Delta}\tanh(\frac{\beta\Delta}{2}) \end{pmatrix}, \qquad |\rho_2\rangle\!\rangle = \begin{pmatrix} 0 \\ \frac{x}{z} \\ 0 \\ 1 \end{pmatrix},$$

$$|\rho_3\rangle\!\rangle = \begin{pmatrix} 0 \\ -\frac{z}{x} \\ -i\frac{\Delta}{2\,x} \\ 1 \end{pmatrix}, \qquad |\rho_4\rangle\!\rangle = \begin{pmatrix} 0 \\ -\frac{z}{x} \\ i\frac{\Delta}{2\,x} \\ 1 \end{pmatrix}. \tag{C8}$$

In matrix notation they read

$$\hat{\rho}_1 = \begin{pmatrix} \frac{1}{2} - \frac{z\tanh(\frac{\beta\Delta}{2})}{\Delta} & -\frac{x\tanh(\frac{\beta\Delta}{2})}{\Delta} \\ -\frac{x\tanh(\frac{\beta\Delta}{2})}{\Delta} & \frac{1}{2} + \frac{z\tanh(\frac{\beta\Delta}{2})}{\Delta} \end{pmatrix} = \frac{e^{-\beta\hat{\mathrm{H}}_{\mathrm{LZ}}}}{\mathrm{Tr}(e^{-\beta\hat{\mathrm{H}}_{\mathrm{LZ}}})}, \tag{C9}$$

$$\hat{\rho}_2 = \frac{1}{\sqrt{2}}\begin{pmatrix} 1 & \frac{x}{z} \\ \frac{x}{z} & -1 \end{pmatrix}, \tag{C10}$$

$$\hat{\rho}_3 = \frac{1}{\sqrt{2}}\begin{pmatrix} 1 & -\frac{z}{x} - \frac{1}{2}\frac{\Delta}{x} \\ -\frac{z}{x} + \frac{1}{2}\frac{\Delta}{x} & -1 \end{pmatrix}, \tag{C11}$$

$$\hat{\rho}_4 = \frac{1}{\sqrt{2}}\begin{pmatrix} 1 & -\frac{z}{x} + \frac{1}{2}\frac{\Delta}{x} \\ -\frac{z}{x} - \frac{1}{2}\frac{\Delta}{x} & -1 \end{pmatrix}. \tag{C12}$$

It can be seen that $\mathrm{Tr}(\hat{\rho}_{2,3,4}) \neq 1$, and hence $\hat{\rho}_{2,3,4}$ can not be interpreted as states. The Liouvillian gap is given by

$$\Delta_{\mathrm{L}} = \min\{|l_2|, |l_3|\}, \tag{C13}$$

where

$$|l_2| = \sqrt{\lambda_2\lambda_2^*} = \sqrt{[\gamma(-\Delta)+\gamma(\Delta)]^2} = 2\pi g^2\Delta\coth(\frac{\beta\Delta}{2})$$
$$= 4\pi g^2 T + \frac{1}{3}\pi g^2\frac{1}{T}\Delta^2 + \mathcal{O}(\Delta^4), \tag{C14}$$

$$|l_3| = \sqrt{\lambda_3\lambda_3^*} = \sqrt{\frac{1}{4}\left[\gamma(-\Delta)+\gamma(\Delta)\right]^2 + \Delta^2}$$
$$= 2\pi g^2 T + \frac{3+2\pi^2 g^4}{12\pi g^2}\frac{1}{T}\Delta^2 + \mathcal{O}(\Delta^3). \tag{C15}$$

The left eigenvectors of the Liouvillian are defined by

$$\langle\!\langle l_m|\mathcal{L} = \lambda_m\langle\!\langle l_m| \iff \mathcal{L}^\dagger|l_m\rangle\!\rangle = l_m^*|l_m\rangle\!\rangle, \tag{C16}$$

and therefore we find for the left eigenvectors

$$\langle\!\langle l_1| = \begin{pmatrix} 1, & 0, & 0, & 0 \end{pmatrix}, \tag{C17}$$

$$\langle\!\langle l_2| = \begin{pmatrix} -\frac{\Delta}{2\,z}\frac{\gamma(-\Delta)-\gamma(\Delta)}{\gamma(-\Delta)+\gamma(\Delta)}, & \frac{x}{z}, & 0, & 1 \end{pmatrix}$$
$$= \begin{pmatrix} \frac{\Delta}{2\,z}\tanh(\frac{\beta\Delta}{2}), & \frac{x}{z}, & 0, & 1 \end{pmatrix}, \tag{C18}$$

$$\langle\!\langle l_3| = \begin{pmatrix} 0, & -\frac{z}{x}, & i\frac{\Delta}{2\,x}, & 1 \end{pmatrix}, \tag{C19}$$

$$\langle\!\langle l_4| = \begin{pmatrix} 0, & -\frac{z}{x}, & -i\frac{\Delta}{2\,x}, & 1 \end{pmatrix}. \tag{C20}$$

We can normalize the first left eigenvector such that in matrix notation we have $\langle\!\langle \varpi_1 | \rho \rangle\!\rangle = \mathrm{Tr}(\hat{1}\hat{\rho}) = \mathrm{Tr}(\hat{\rho}) = 1$, i.e., $\langle\!\langle \varpi_1| = \begin{pmatrix} \sqrt{2}, & 0, & 0, & 0 \end{pmatrix}$, and thus we get

$$\hat{\varpi}_1 = \begin{pmatrix} 1 & 0 \\ 0 & 1 \end{pmatrix} \tag{C21}$$

$$\hat{\varpi}_2 = \frac{1}{\sqrt{2}}\begin{pmatrix} 1 + \frac{\Delta}{2\,z}\tanh(\frac{\beta\Delta}{2}) & \frac{x}{z} \\ \frac{x}{z} & -1 + \frac{\Delta}{2\,z}\tanh(\frac{\beta\Delta}{2}) \end{pmatrix}, \tag{C22}$$

$$\hat{\varpi}_3 = \frac{1}{\sqrt{2}}\begin{pmatrix} 1 & -\frac{z}{x} + \frac{1}{2}\frac{\Delta}{x} \\ -\frac{x}{z} - \frac{1}{2}\frac{\Delta}{x} & -1 \end{pmatrix}, \tag{C23}$$

$$\hat{\varpi}_4 = \frac{1}{\sqrt{2}}\begin{pmatrix} 1 & -\frac{z}{x} - \frac{1}{2}\frac{\Delta}{x} \\ -\frac{x}{z} + \frac{1}{2}\frac{\Delta}{x} & -1 \end{pmatrix}. \tag{C24}$$

Further, we may normalize the left and right eigenvectors such that they form a complete and orthonormal basis,

$$\langle\!\langle L_n | R_m \rangle\!\rangle = \delta_{nm}, \qquad \sum_n |R_n\rangle\!\rangle\langle\!\langle L_n| = \hat{1}, \tag{C25}$$

and thus we have

$$|R_1\rangle\!\rangle = \begin{pmatrix} \frac{1}{\sqrt{2}} \\ -\sqrt{2}\frac{x}{\Delta}\tanh(\frac{\beta\Delta}{2}) \\ 0 \\ -\sqrt{2}\frac{z}{\Delta}\tanh(\frac{\beta\Delta}{2}) \end{pmatrix}, \qquad |R_2\rangle\!\rangle = \frac{2z}{\Delta}\begin{pmatrix} 0 \\ \frac{x}{z} \\ 0 \\ 1 \end{pmatrix},$$

$$|R_3\rangle\!\rangle = \sqrt{2}\frac{x}{\Delta}\begin{pmatrix} 0 \\ -\frac{z}{x} \\ -i\frac{1}{2}\frac{\Delta}{x} \\ 1 \end{pmatrix}, \qquad |R_4\rangle\!\rangle = \sqrt{2}\frac{x}{\Delta}\begin{pmatrix} 0 \\ -\frac{z}{x} \\ i\frac{1}{2}\frac{\Delta}{x} \\ 1 \end{pmatrix}$$

$$\langle\!\langle L_1| = \begin{pmatrix} \sqrt{2}, & 0, & 0, & 0 \end{pmatrix},$$

$$\langle\!\langle L_2| = \frac{2z}{\Delta}\begin{pmatrix} \frac{1}{2}\Delta\frac{1}{z}\tanh(\frac{\Delta}{2}\beta), & \frac{x}{z}, & 0, & 1 \end{pmatrix},$$

$$\langle\!\langle L_3| = \sqrt{2}\frac{x}{\Delta}\begin{pmatrix} 0, & -\frac{z}{x}, & i\frac{1}{2}\Delta\frac{1}{x}, & 1 \end{pmatrix},$$

$$\langle\!\langle L_4| = \sqrt{2}\frac{x}{\Delta}\begin{pmatrix} 0, & -\frac{z}{x}, & -i\frac{1}{2}\frac{\Delta}{x}, & 1 \end{pmatrix}. \tag{C26}$$

Appendix D: Lindbladian master equation

The equation describing the time evolution of the reduced density matrix $\hat{\rho}$, is a linear and time-local master equation, given by

$$\partial_t\hat{\rho} = \widehat{\mathcal{L}}(t)\hat{\rho}, \tag{D1}$$

where $\widehat{\mathcal{L}}(t)$ is the Liouvillian written in Lindblad form (see main text). In the basis $\{\hat{\Gamma}_i\}_{i=1}^4 = \frac{1}{\sqrt{2}}\{\hat{1}, \hat{\sigma}^x, \hat{\sigma}^y, \hat{\sigma}^z\}$, where the vector representation of $\hat{\rho}(t)$ reads $|\rho(t)\rangle\!\rangle = \sum_{i=1}^4 c_i(t)|\Gamma_i\rangle\!\rangle$, Eq. (D1) takes the form

$$\partial_t c_1(t) = 0, \tag{D2}$$

$$\partial_t c_2(t) = -4\pi g^2 x c_1(t) - 2\pi g^2 \coth[\beta b(t)]\frac{x^2 + b^2(t)}{b(t)} c_2(t) - 2z(t)c_3(t) - 2\pi g^2 \coth[\beta b(t)]\frac{x\, z(t)}{b(t)} c_4(t), \tag{D3}$$

$$\partial_t c_3(t) = 2z(t)c_2(t) - 2\pi g^2 \coth[\beta b(t)] b(t) c_3(t) - 2x c_4(t), \tag{D4}$$

$$\partial_t c_4(t) = -4\pi g^2 z(t) c_1(t) - 2\pi g^2 \coth[\beta b(t)]\frac{x\, z(t)}{b(t)} c_2(t) + 2x\, c_3(t) - 2\pi g^2 \coth[\beta b(t)]\frac{b^2(t) + z^2(t)}{b(t)} c_4(t), \tag{D5}$$

with $b(t) \equiv \sqrt{x^2 + z^2(t)}$. We numerically solved the above equations to find $|\rho(t)\rangle\!\rangle$.

[1] I. Bloch, Nat. Phys. **1**, 23 (2005).
[2] I. Bloch, J. Dalibard, and W. Zwerger, Rev. Mod. Phys. **80**, 885 (2008).
[3] I. Bloch, J. Dalibard, and S. Nascimbene, Nat. Phys. **8**, 267 (2012).
[4] S. Lloyd, Nature (London) **406**, 1047 (2000).
[5] E. Farhi, J. Goldstone, S. Gutmann, J. Lapan, A. Lundgren, and D. Preda, Science **292**, 472 (2001).
[6] M. Nielsen and I. L. Chuang, *Quantum Computation and Quantum Information* (Cambridge University Press, Cambridge, UK, 2000).
[7] R. P. Feynman, Int. J. of Theo. Phys., **21**, 467 (1982).
[8] V. S. Denchev, S. Boixo, S. V. Isakov, N. Ding, R. Babbush, V. Smelyanskiy, J. Martinis, and H. Neven, Phys. Rev. X **6**, 031015 (2016).
[9] S. Boixo, V. N. Smelyanskiy, A. Shabani, S. V. Isakov, M. Dykman, V. S. Denchev, M. Amin, A. Smirnov, M. Mohseni, and H. Neven, Nat. Commun. **7** 10327 (2016).
[10] T. Lanting *et al.*, Phys. Rev. X **4**, 021041 (2014).
[11] N. G. Dickson *et al.*, Nat. Commun. **4**, 1903 (2013).
[12] M.W. Johnson *et al.*, Nature (London) **473**, 194 (2011).
[13] T. Albash and D. A. Lidar, arXiv:1611.04471, (2016).
[14] B. Damski, Phys. Rev. Lett. **95**, 035701 (2005).
[15] B. Damski and W. H. Zurek, Phys. Rev. A **73**, 063405 (2006).
[16] J. Dziarmaga, Adv. Phys. **59**, 1063 (2010).
[17] A. del Campo and W. H. Zurek, Int. J. Mod. Phys. **29**, 1430018 (2014); A. del Campo, G. De Chiara, G. Morigi, M. B. Plenio, and A. Retzker, Phys. Rev. Lett. **105**, 075701 (2010); K. Pyka, J. Keller, H. L. Partner, R. Nigmatullin, T. Burgermeister, D. M. Meier, K. Kuhlmann, A Retzker, M. B. Plenio, W. H. Zurek, A. del Campo, and T. E. Mehlstübler, Nat. Commun. **4**, 2291 (2013); S. Ulm, J. Roßnagel, G. Jacob, C. Degünther, S. T. Dawkins, U. G. Poschinger, R. Nigmatullin, A. Retzker, M. B. Plenio, F. Schmidt-Kaler, and K. Singer, Nat. Commun. **4**, 2290 (2013); D. Chen, M. White, C. Borries, and B. DeMarco, Phys. Rev. Lett. **106**, 235304 (2011); G. Lamporesi, S. Donadello, S. Serafini, F. Dalfovo, and G. Ferrari, Nat. Phys. **9**, 656 (2013).
[18] A. Polkovnikov, Phys. Rev. B **72**, 161201(R) (2005).
[19] C. De Grandi, V. Gritsev, and A. Polkovnikov, Phys. Rev. B **81**, 012303 (2010).
[20] Messiah, A., (1962), *Quantum Mechanics, Vol. II* (North-Holland Publishing Company, Amsterdam).
[21] T. W. B. Kibble, J. Phys. A **9**, 1387 (1976).
[22] T. W. B. Kibble, Phys. Rep. **67**, 183 (1980).
[23] W. Zurek, Nature (London) **317**, 505 (1985).
[24] W. Zurek, Acta Phys. Pol. B **24**, 1301 (1993).
[25] W. Zurek, Phts. Rep. **276**, 177 (1996).
[26] T. Kato, J. Phys. Soc. Jpn. **5**, 435 (1950).
[27] L.D. Landau, Zur Theorie der Energieübertragung. II, Phys. Z. Sowjetunion **2**, 46 (1932).
[28] C. Zener, Non-adiabatic crossing of energy levels, Proc. R. Soc. A **137**, 696 (1932).
[29] E. C. G. Stueckelberg, Theorie der unelastischen Stösse zwischen Atomen, Helv. Phys. Acta **5**, 369 (1932).
[30] E. Majorana, Atomi orientati in campo magnetico variabile, Nuovo Cimento **9**, 43 (1932).
[31] N. V. Vitanov and B. M. Garraway, Phys. Rev. A **53**, 4288 (1996).
[32] S. Jansen, M.-B. Ruskai, and R. Seiler, J. Math. Phys. **48**, 102111 (2007).
[33] G. Rigolin, G. Ortiz, and V. H. Ponce, Phys. Rev. A **78**, 052508 (2008).
[34] L. Campos Venuti, T. Albash, D. A. Lidar, and P. Zanardi, Phys. Rev. A **93**, 032118 (2016).
[35] J. E. Avron, M. Fraas, G. M. Graf, and P. Grech, Commun. Math. Phys. **314**, 163 (2012).
[36] E. Lieb, T. Schultz, and D. Mattis, Ann. Phys. (NY) **16**, 407 (1961).
[37] P. Pfeuty, Ann. Phys. (NY) **57**, 79 (1970).
[38] M. Henkel, *Conformal Invariance and Critical Phenomena* (Springer-Verlag Berlin Heidelberg, 1999).

[39] J. Dziarmaga, Phys. Rev. Lett. **95**, 245701 (2005).
[40] R. W. Cherng and L. S. Levitov, Phys. Rev. A **73**, 043614 (2006).
[41] E. B. Davies, Commun. Math. Phys. **39**, 91 (1974).
[42] T. Albash, S. Boixo, D. A. Lidar, and P. Zanardi, New J. Phys. **14**, 123016 (2012).
[43] A. Kossakowski, A. Frigerio, V. Gorini, and M. Verri, Commun. Math. Phys. **57**, 97 (1977); **60**, 96(E) (1978).
[44] H.-P. Breuer and F. Petruccione, *The Theory of Open Quantum Systems* (Oxford University Press, Oxford, 2002).
[45] P. Nalbach, S. Vishveshwara, and A. A. Clerk, Phys. Rev. B **92**, 014306 (2015).
[46] D. Patane, A. Silva, L. Amico, R. Fazio, and G. E. Santoro, Phys. Rev. Lett. **101**, 175701 (2008).
[47] M. Keck, S. Montangero, G. E. Santoro, R. Fazio, and D. Rossini, New J. Phys. 19 113029 (2017).
[48] P. Hedvall and J. Larson, arXiv:1712.01560, (2017).
[49] F. Wilczek and A. Zee, Phys. Rev. Lett. **52**, 2111 (1984).
[50] P. Zanardi and L. Campos Venuti, Phys. Rev. A **91**, 052324 (2015).
[51] W. K. A. Salem, Ann. Henri Poincaré **8**, 569 (2007).